

Fluctuation Phenomena in Neurological Local Field Potentials

A THESIS
SUBMITTED TO THE FACULTY OF THE GRADUATE SCHOOL
OF THE UNIVERSITY OF MINNESOTA
BY

Beth Masimore

IN PARTIAL FULFILLMENT OF THE REQUIREMENTS
FOR THE DEGREE OF
DOCTOR OF PHILOSOPHY

James Kakalios and A. David Redish, Advisors

June, 2008

Acknowledgements

I am in the wonderfully fortunate position of having too many people to possibly thank. This thesis would not exist without the help from many people, both in and out of the lab.

- My advisors, Jim Kakalios and Dave Redish. I still don't know what the initial idea was for this research, but I'm glad that it happened and am grateful for the opportunity to develop the idea and begin an exciting collaboration.
- Neil Schmitzer-Torbert, Jadin Jackson, Adam Johnson, Chris Boldt, Matthijias van der Meer and John Ferguson. From sharing their data with me for new analyses to providing experimental support and instruction, this research could not have happened without them. I feel fortunate that these wonderful collaborators were also wonderful and supportive friends.
- Jamie White, Juniata College. I can't imagine ever making it to graduate school, or even developing an interest in physics, without his support, encouragement and, most importantly, excellent teaching.
- Lindsey Hillesheim, Melissa Eblen-Zayas, and Emily Maher. I'm grateful that they reached out to me early in grad school and provided essential informal mentoring and supportive friendships. Their post grad-school success has already been inspirational.
- Natalia Melcer and Tim Meyer. I had the wonderful opportunity to pursue interests outside of the lab and to develop skills that will facilitate a career transition to work in science policy. Their mentoring, guidance, and friendship provided the necessary motivation to actually finish.
- Kevin Parendo. Aside from myself, he is most responsible for this thesis reaching completion. His love and support are more than I ever could have wished for.

This work was supported by grants from NIH (MH68029-01), an NSF IGERT fellowship (#9870633), a University of Minnesota Graduate School grant for Interdisciplinary Research, Scholarly and Creative Activities, a University of Minnesota Graduate School Grant-in-Aid, and a University of Minnesota Louise T. Dosdall fellowship.

Abstract

The study of noise and fluctuations has proven useful in a wide variety of disordered systems, from disordered condensed matter systems to noisy biological systems. Neurological signals termed local field potentials are characterized by apparently random fluctuations interspersed with periods of clear oscillatory activity. Numerous mathematical theories have been developed that describe the power spectrum that results from different fluctuation phenomena. Several of these theories are presented with discussions of how they may apply to local field potentials in the brain. Experiments and simulations are proposed that could help to clarify specific aspects of the fluctuation origins of local field potentials. Given long time series of neurological voltage fluctuations, it can be difficult to detect the occurrence of oscillatory activity. An analytical method is presented to identify the presence of oscillations within a signal. This method is verified through simulations and experiments on signals with known oscillations. Using this method, a previously unknown oscillation is detected, termed γ_{50} , that is recorded in the striatum of awake, behaving rats. The γ_{50} signal is characterized by short bursts of coherent 50 Hz oscillations, and is found to be correlated with the initiation of movement. Preliminary experiments were conducted to identify the origin of γ_{50} events. Data from these experiments is discussed along with remaining open research questions and future directions.

Table of Contents

Acknowledgments	i
Abstract	ii
Table of Contents	iii
List of Figures	v
1. Introduction	
1.1 Introduction to Electrophysiology.....	1
1.2 Local Field Potentials: A ‘Mesoscopic’ Phenomena.....	3
1.3 Approaches to Studying Local Field Potentials.....	5
2. Statistical Analysis of Noise	
2.1 Introduction.....	10
2.2 Random Signals.....	11
2.3 Modeling Physical Systems.....	14
2.4 Noise and Local Field Potentials.....	15
2.4.1 Current Theory of Local Field Potential Origin.....	15
2.4.2 Gaps in the Theory.....	16
2.4.3 Potential Benefits of Noise Analysis.....	17
3. Power Spectra of Local Field Potentials	
3.1 Introduction.....	19
3.2 Distribution of Poisson Fluctuators.....	19
3.3 Frequency Filtering Properties of Dielectric Media.....	25
3.4 Self-Organized Criticality.....	29
4. Experimental Methods	
4.1 Brain Structures.....	33
4.1.1 Hippocampus.....	33
4.1.2 Postsubiculum.....	34
4.1.3 Striatum.....	34
4.2 Animals.....	35
4.3 Behavioral Tasks.....	35

4.4 Neural Recording.....	39
4.5 Surgery.....	41
4.5 Position and Velocity.....	41
5. Analytical Technique	
5.1 Introduction.....	43
5.2 Overview of Technique.....	43
5.3 Analysis Methods.....	44
5.4 Results.....	45
5.4.1 Simulation.....	46
5.4.2 Hippocampus.....	49
5.4.3 Postsubiculum (cortex).....	50
5.4.1 Striatum.....	52
5.5 Discussion.....	54
5.5.1 Importance for Other Recording Technologies	55
5.5.2 Detection of Non-Neural Noise Sources.....	55
5.5.3 Relation to Coherence.....	56
5.5.4 Relation to Bispectral Analysis.....	56
5.5.5 The Choice of Spectral Estimation Techniques	57
5.6 Conclusions.....	58
6. 50 Hz Oscillations	
6.1 Introduction.....	59
6.2 Cross-Frequency Self Correlations.....	59
6.3 Behavioral Correlations of γ 50 Events.....	61
6.4 Conclusions.....	66
7. Future Directions and Open Questions	
7.1 Introduction.....	67
7.2 Fluctuator Simulation.....	67
7.3 Dielectric Properties of Brain Tissue.....	68
7.4 Self-Organized Criticality.....	69
7.5 Relation to Other Dynamic Neural Signals.....	70

7.6 γ 50 Oscillations.....	70
7.6.1 Origin of Oscillations.....	70
7.6.2 Dopamine.....	74
8. Summary.....	79
References.....	80

List of Figures

Chapter 1

1.1 Sample Power Spectra.....	5
1.2 Hippocampal Theta Rhythm.....	8
1.3 Coherent Oscillation.....	8

Chapter 2

2.1 Random Signals.....	12
2.2 Autocorrelation of Random Signals.....	13
2.3 Power Spectra of Random Signals.....	14

Chapter 3

3.1 Poisson Fluctuator.....	20
3.2 Statistical Properties of a Poisson Flucator.....	21
3.3 Autocorrelation and Power Spectrum of a Poisson Fluctuator.....	22
3.4 Simulation of 1/f Noise.....	23

Chapter 4

4.1 Linear Track Task.....	36
4.2 Open Field and Open Field Goal Tasks	36
4.3 Nose Poke Task.....	37
4.4 Multiple-T Task	38
4.5 Take-5 Task	39
4.6 Tetrode Schematic	40

Chapter 5

5.1 Simulation.....	48
5.2 Correlation Structure of LFPs Recorded from the Hippocampus of Two Rats.....	50
5.3 Correlation Structure of LFPs Recorded from the Postsubiculum of Two Rats.....	52
5.4 Correlation Structure of LFPs Recorded from the Dorsocentral Striatum of Five Rats.....	53

Chapter 6

6.1 Cross-Frequency Self Correlation.....60
6.2 Example γ 50 Event from the Multiple-T Task.....63
6.3 Example γ 50 Event from the Take-5 Task.....64
6.4 Speed Relative to the Time of γ 50 Events.....65

Chapter 7

7.1 Recording Locations.....73
7.2 Preliminary Data of Dopamine Manipulations.....77

Chapter 1

Introduction

1.1 Introduction to Electrophysiology

Our understanding of animal and human nervous systems has changed significantly across decades and centuries, with ever improving technologies making new levels of nervous system function accessible to researchers. Early research was confined to clinical studies in which large sections of the brain were altered by either injury or disease. We have quickly progressed to a point where many levels of neuronal function are accessible to researchers, ranging from molecules and proteins through single cells and cell groups, to methods for quantifying and analyzing large scale behaviors.

A standard way to study various properties of neural systems is through electrophysiology. Electrophysiology is the study of the electrical properties of biological cells and tissues. It involves measurements of voltage change or electrical current flow on a wide variety of scales from single ion channel proteins to whole tissues like the brain.

One of the most familiar of electrophysiological techniques is the electroencephalogram, or EEG. The EEG is a record of electric potential fluctuations recorded from electrodes on the scalp.¹ The scalp electrode measures fields due to neural activity in tissue volumes containing $10^8 - 10^9$ neurons and it is primarily the electrical activity that occurs at the synapse between neurons that contributes to the EEG signal. The dominant contribution to the EEG signal comes from the brain structure closest to the surface, cortex. This is due to the strong spatial drop off in the magnitude of electric

fields. In addition to its surface location, the cellular architecture of the cortex makes it particularly conducive to being recorded at some distance. Neurons within cortex are arranged in layers that parallel the skull, with the main axis of the neurons radial to the skull. The electrical currents that relate to the synaptic electrical fluctuations are along the main axis of the neuron, thus also radial to the skull. This arrangement results in many electrical currents in the same direction such that any coherent activity will persist through the spatial averaging that occurs in EEG recordings.

This technique has been available for nearly a century and its noninvasive nature has provided researchers with a powerful window to the workings of the brain. Activity within the EEG has been associated with various states of consciousness and cognitive processes. For example, the eyes-closed awake state, termed the *alpha state*, shows widespread near sinusoidal oscillation at 10 Hz. Deep sleep is characterized by larger amplitude activity at lower frequencies. Most people are familiar with EEG from its use in clinical settings, where it can be used for the identification of deep anesthesia, seizures, and some neurological disorders. In the psychology research setting, researchers have identified EEG correlations with cognitive processes associated with mental calculations, working memory, and selective attention.

Another way to study various properties of neural systems is to record the electrical activity by placing electrodes within the extracellular medium. A variety of biomechanical processes underlie the fluctuations observed in this signal. The low-frequency portion of this signal (where low frequency here is approximately 1 – 500Hz) is called the local field potential (LFP) and, like EEG, is believed to reflect the electrical

fluctuations occurring at synapses between neurons. The spatial range of fluctuators that are thought to comprise this portion of the signal is of an order that includes hundreds of neurons. For this reason, local field potentials are thought to reflect the activity of local populations of neurons.²

As mentioned, local field potentials are the low frequency portion of the signal recorded from electrodes placed in the extracellular medium. The high-frequency portion of this signal (typically 600 – 6000 Hz) can be recorded and analyzed to identify neural spikes. During the normal, resting state, neurons maintain a potential difference between the inside and outside of the cell. *Action potentials* are defined as discrete events in which the polarization across the cell membrane reverses and then returns to the resting state. During this process, there are several ionic currents in the extracellular space that result in measurable potential changes, commonly referred to as *spikes*. These discrete events last several milliseconds and by recording at a high rate, researchers can capture both the timing of events as well as the unique waveform of the potential change.

1.2 Local Field Potentials: A ‘Mesoscopic’ Phenomena

While there are many open questions to occupy EEG researchers for the foreseeable future, there is also a stable and robust foundation of theoretical, computational, and experimental work in this field. Given the similarities between EEG and LFP, there has been a tendency to extrapolate the theoretical framework of EEG to LFPs. For some situations, this extrapolation provides useful insights with a minimum of problems. For example, LFPs in cortex are likely well described with the same theory as EEG as this theory is based upon assumptions true of cortical anatomy. In other

situations, this theoretical transfer breaks down. EEG are recorded from the scalp surface, thus outside the electrically active region although LFPs are recorded from within the active region. When recording from outside the scalp, electrical signals experience significant spatial averaging as a result of volume conduction. This results in the recorded signal being relatively insensitive to parameters such as electrode size and location. Local fields experience a much lesser amount of spatial averaging and thus the recorded signal is extremely sensitive to electrode parameters.

Another approach to interpreting LFPs is to assume that spikes are the fundamental neural fluctuation and that local field potentials uniquely correlate with spike activity. As mentioned, the extracellular spikes relate to cellular action potentials. These action potentials occur when the synaptic inputs to the cell reach a critical threshold that triggers the event. The synaptic inputs that sum to trigger action potentials are the same synaptic events that are thought to underlie LFPs, thus it is reasonable to anticipate a correlation between spikes and LFPs. For the purposes of modeling, some researchers have assumed that LFPs can be reconstructed from spike activity by assuming a single synaptic event occurred congruent with each spike and that the synaptic event had a particular form.³ While these assumptions have some physiological basis, they fail to acknowledge the complexity of subthreshold activity.^{4,5}

As is the case in many multi-scale scientific fields, it's becoming clear that theories that were developed for one spatial scale often break down when applied to others. Just as the case of superfluidity, where an understanding of the atomic structure of helium is necessary but not sufficient to understand the phenomena, local field potentials

possess many of the characteristics of a mesoscale system and thus warrant dedicated research attention.

1.3 Approaches to Studying Local Field Potentials

Local field potentials have been well studied in some areas of the brain while they are still relatively unexplored in others. The data obtained in a local field potential experiment is a long time series of voltages – perhaps 30 minutes of data recorded at 2000 Hz - which makes examination in the temporal domain intractable. Alternatively, one can study the signal in the frequency domain and the standard first approach to characterize a long time series is to examine the power spectrum. Examples of power spectra of LFPs recorded from several different brain structures are shown in Figure 1.1. Mathematical aspects of the power spectrum will be discussed in Chapter 2 and experimental details regarding these data will be discussed in Chapter 3.

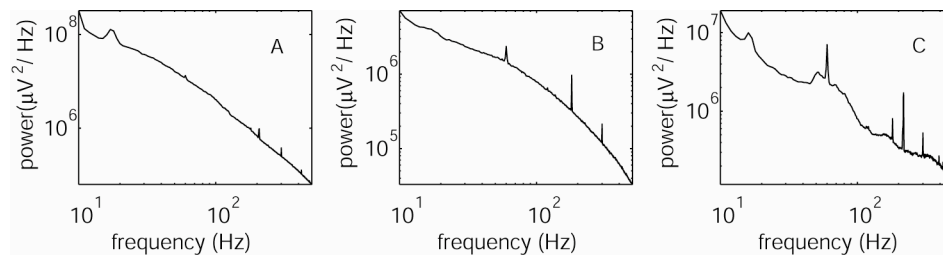


Figure 1.1 Sample Power Spectra

Power spectra of local field potentials recorded from different brain structures. Panel A is the power spectrum of an LFP recording from hippocampus and shows a slope of -2.2. Panel B is the power spectrum of an LFP recording from motor cortex and shows an average slope of -1.5 . Panel C is the power spectrum of an LFP recording from ventral striatum and shows an average slope of -1.1.

These power spectra show several qualitative features. As displayed on logarithmic axes, the power spectra all appear approximately linear with slopes ranging

from -2.2 for that in figure 1.1.A to -1.1 for that shown in figure 1.1.C. The deviations away from linearity also vary. Both figures 1.1.A and 1.1.B can be fit to a line but may be better described by a function that acknowledges the slow curvatures. The deviations from linearity present in figure 1.1.C are more local in nature; there are various bumps around a generally linear trend. All of the spectra show very sharp peaks that are due to external electrical noise rather than any type of neural activity.

None of these qualitative features are terribly surprising given both a general knowledge of fluctuation phenomena and fundamental neural physiology. A wide variety of systems, both biological and non-biological, exhibit power law spectral behavior. Perhaps the most well studied system is voltage fluctuations in condensed matter systems ranging from metals to vacuum tubes to carbon resistors.⁶ Famous reviews of $1/f$ noise cover topics ranging from noise in traffic flow to fluctuations in undersea currents.^{6,7} In the biological realm, power law fluctuations have been identified in systems ranging from current fluctuations across cellular membranes to large scale physiological parameters such as heart rate variability in healthy adults.^{8,9} Another signal of particular relevance is the EEG which has also been shown to exhibit $1/f$ noise.^{10,11}

Although the nature of scientific reporting makes it difficult to report on negative findings, a cursory literature search leaves a person wondering if there are systems whose power spectra do not exhibit a power-law frequency dependence and questioning what can be gained by identifying yet another system with this characteristic. The general utility of noise measurements will be discussed in Chapter 2 along with a discussion of the possible benefit of such measurements of local field potentials. Many mathematical

models have been developed to explain the $1/f$ noise found in a wide range of systems. Chapter 3 will focus on possible ways to map several of these models onto LFPs.

Another qualitative feature of the power spectra shown in Figure 1.1 is the deviations away from linearity. The existence of bumps on the power spectra is not terribly surprising. Different brain structures are known to display different oscillatory states, termed *fundamental frequencies* and these epochs of oscillatory activity appear in the power spectrum as small, localized bumps of high power. For example, in the hippocampus, a brain structure involved in learning and memory, there are two well characterized oscillations. Oscillations that occur at 6-10 Hz are labeled theta oscillations and persist for up to minutes, while the animal is engaged in attentive behaviors.^{12, 13} During periods of rest and autonomous behaviors, this strong 6-10 Hz oscillation is not present and the activity is largely irregular, even being referred to as Large Irregular Activity (LIA). These epochs of LIA are punctuated by 160-200 Hz oscillations known as sharp waves. Sharp waves are characterized by ripples at the given frequency with a characteristic duration of 100 ms.¹⁴ The cortex typically shows 40 Hz oscillations while a variety of structures show oscillations in the range of 10-70 Hz, collectively referred to as beta or gamma oscillations.¹⁵ Figure 1.2 shows activity recorded from rodent hippocampus where one can see theta activity (8 Hz) emerging from irregular activity.

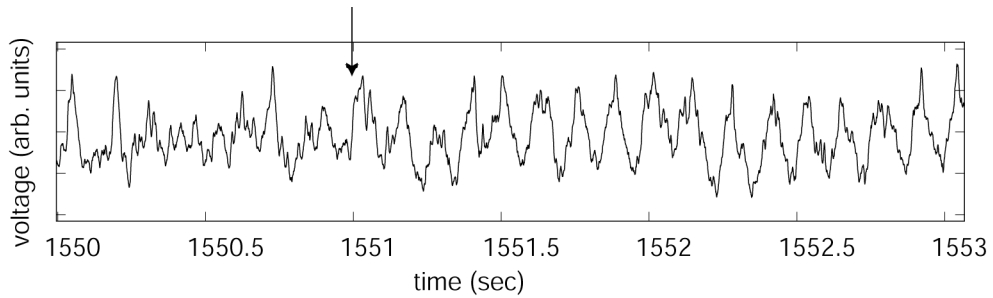


Figure 1.2 Hippocampal Theta Rhythm

Local field potential recorded from rat hippocampus showing theta emerging from irregular activity. The 8Hz rhythm begins at approximate 1551 sec (indicated by arrow) and continues through the rest of the trace.

A typical experiment involves multiple electrodes placed within the same brain structure. The signals recorded from these different locations can be compared to gain additional information. Some types of oscillatory events occur over an entire brain region, and when the recorded oscillation is in phase across multiple signals, it is referred to as a *coherent oscillation*. An example of such an event is shown in figure 1.3.

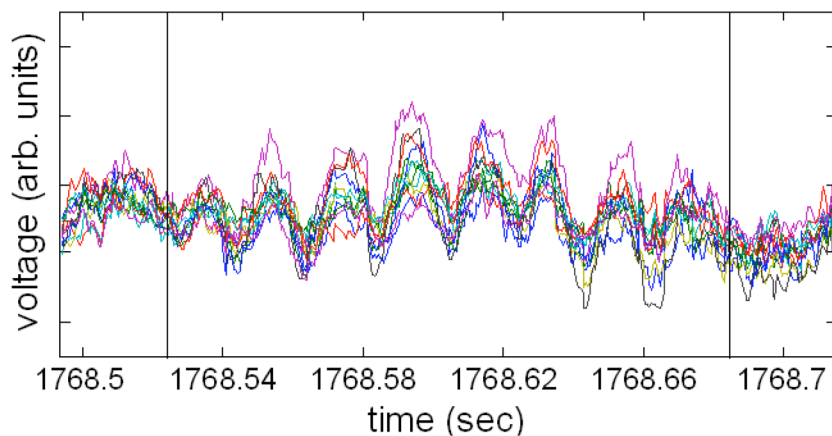


Figure 1.3: Coherent Oscillation

Raw LFP data where the individual lines are raw LFP signals recorded from different electrodes in a single animal. The two vertical lines indicate the identified oscillatory event.

This dissertation is organized as follows. Chapter 2 provides theoretical background for statistical analysis of fluctuation phenomena, while chapter 3 applies this analysis to neurological local field potentials. Following an overview of experimental techniques in chapter 4, chapters 5 and 6 will discuss aspects of the bumps in the power spectrum. Specifically, a technique for identifying the frequency range of interesting features will be presented in chapter 5 and the behavioral significance of a newly identified feature will be discussed in chapter 6.

Chapter 2

Statistical Analysis of Noise

2.1 Introduction

A common type of experiment among many disparate scientific disciplines is to repeatedly measure a particular variable and then analyze the recorded fluctuations about an average value. A physicist might measure the current across a superconducting film, while a geologist might measure the flood level of the Nile River, and a neuroscientist might measure the voltage fluctuations in the cortex of a monkey performing a task. These scientists will describe their data differently – one referring to the recorded fluctuations as noise, while another describes the data as a fluctuating signal. In each case, the scientist has recorded a time series of a macroscopic variable and may wish to understand the microscopic phenomena that give rise to the variations of the macroscopic variable. Studying the fluctuations, or noise, provides one framework to possibly link the microscopic and macroscopic regimes.

As mentioned in Chapter 1, it is widely believed that local field potentials reflect the electrical fluctuations that occur at the synapses between neurons. Several experimental studies support this hypothesis within certain brain structures but the hypothesis is also incomplete. Analyzing local field potentials from the perspective of noise and fluctuations could help to complete the link from microscopic fluctuations to macroscopic observations. Even if this link proves elusive, there are several ways in which noise analyses could prove useful.

2.2 Random Signals

The fluctuations considered here will be those that appear as time series of a continuous variable, as opposed to those that can be described as a fluctuating two state system or a point process. Three such example time series are shown in Figure 2.1. The time series in Figure 2.1.A was generated by drawing random numbers from a Gaussian distribution; each value is independent of all others. The second time series, displayed in Figure 2.1.B, was generated by superimposing many ($n = 85$) two state fluctuators, each governed by Poisson statistics, with an exponential distribution of Poisson rates. This particular time series will be discussed in greater detail in chapter 3. The time series in Figure 2.1.C is that of a random walk; from an initial location, the position of the next point is chosen at random. All of these signals could be described as random but there are clear qualitative differences between them. Aspects of these qualitative differences can be quantified.

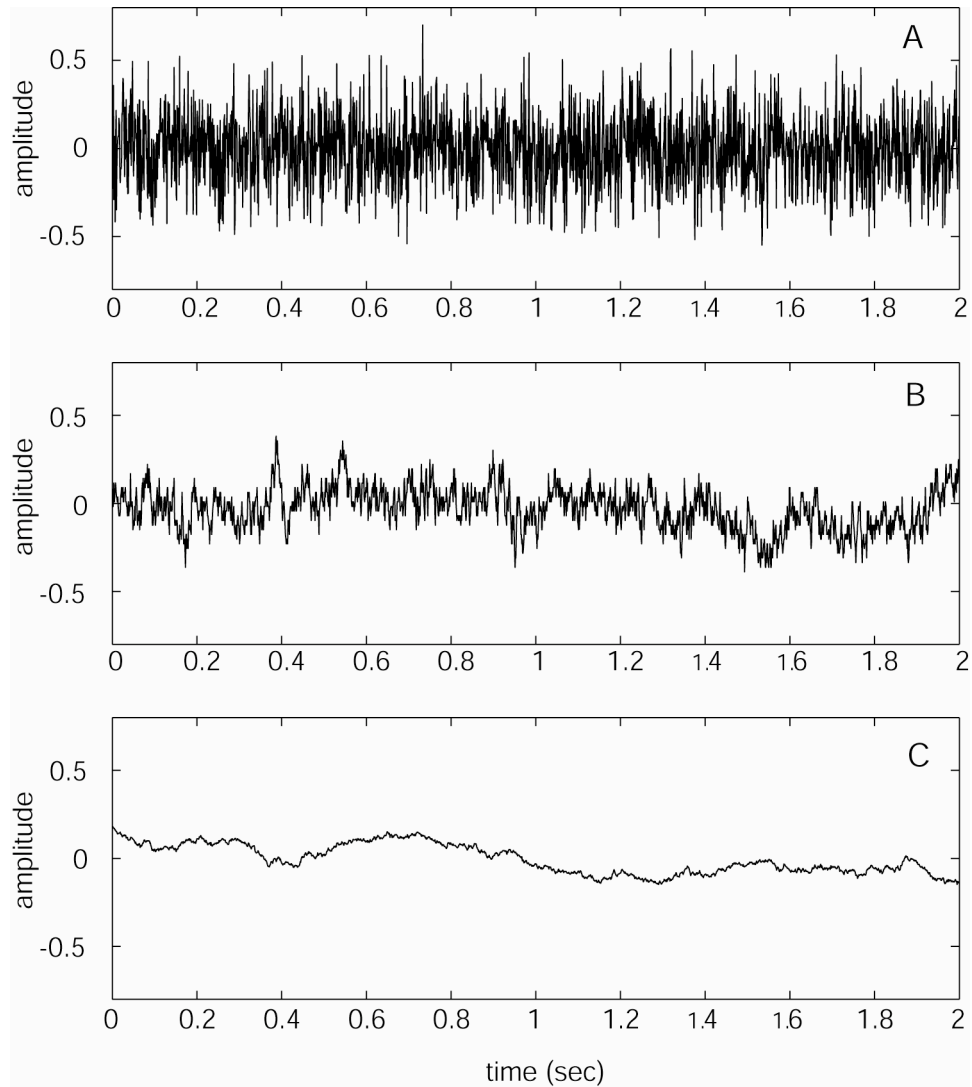


Figure 2.1 Random Signals

Three signals generated by different random methods. (A) Gaussian white noise obtained by selecting numbers at random from a normal distribution; each value is independent of the others. (B) A random time series generated by superimposing 85 two state Poisson fluctuators. (C) Brown noise generated through a random walk. Each value is obtained by adding a Gaussian random number to the previous value.

The two point autocorrelation function provides one quantitative measure of these differences in randomness, by determining how well a signal correlates with a time shifted copy of itself. Autocorrelation functions for the signals shown above are

displayed in figure 2.2. A quickly varying signal such as that shown in Figure 2.1.A exhibits an autocorrelation function that decays to zero nearly instantaneously indicating that knowledge of the signal at a particular time provides no predictive value of the signal at a later time. Slowly varying signals, such as that shown in Figure 2.1.C, show an autocorrelation function that decays to zero very slowly. Signals such as that shown in Figure 2.1.B possess some intermediate amount of correlation and the autocorrelation function decays at some intermediate rate.

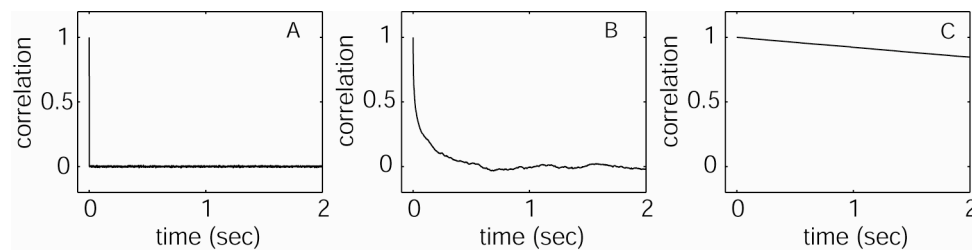


Figure 2.2 Autocorrelation of Random Signals

Autocorrelation functions of the signals shown in figure 2.1. (A) Gaussian white noise signals show autocorrelations that immediately drop to zero as there is no correlation between values. (B) This signal shows an autocorrelation that decays at an intermediate rate. (C) This signal shows a high amount of correlation with the autocorrelation decaying very slowly.

While the autocorrelation function provides a useful quantitative measure of randomness in a somewhat intuitive way, an alternative technique is often more analytically useful. The power spectrum, given by the square of the Fourier transform coefficients of the time series, gives an estimate of the ‘power’ carried by each frequency. Depending on the dimensionality of the time series, the power spectrum may represent the actual physical power in the signal or it may be a conceptually similar quantity. For many time series, including the three presented here, the power spectrum can be well

described by $S = \frac{1}{f^\alpha}$, where S is the power, f is frequency and α is a constant. The constant can be easily determined by plotting the frequency dependence of the power spectrum on logarithmic axes and finding the slope of the line, as shown in Figure 2.3. As can be seen, the power spectrum of the first signal (Fig 2.1.A), for which the autocorrelation decays to zero instantaneously, is flat across all frequencies. The time series with the intermediate amount of correlation (Fig. 2.1.B) shows a power spectrum with a slope near -1 while the highly correlated time series (Fig. 2.1.C) shows a power spectrum with a slope near -2.

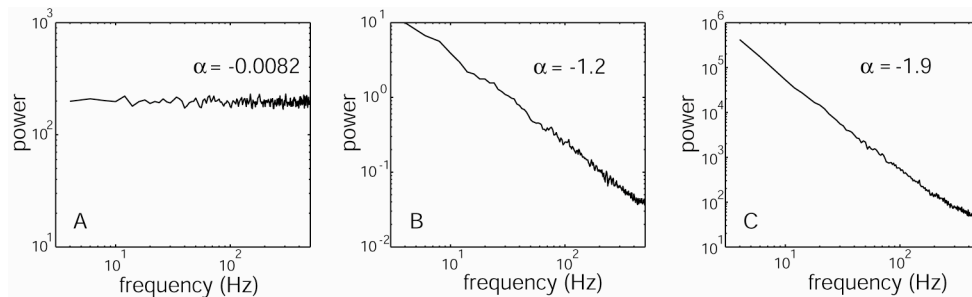


Figure 2.3 Power Spectra of Random Signals

Power spectra of the signals show in figure 2.1. (A) The Gaussian white noise signal shows a flat power spectrum, with equal power at all frequencies. (B) This intermediate signal shows a power spectrum with a slope of -1. (C) This Brownian signal shows a power spectrum with a slope of -2.

2.3 Modeling Physical Systems

For the three classes of signals discussed above, the autocorrelation results and power spectra frequency dependencies can all be derived analytically. The utility of fluctuation study becomes apparent when these mathematical constructs are mapped onto a physical substrate. Assuming that the dimensionality of the time series shown in figure 2.1 is that of current, all of the signals could arise from common (or only mildly

contrived) electronic fluctuations in certain solids. The uncorrelated noise in figure 2.1.A could be that of thermal noise across a standard carbon resistor.^{16, 17} The moderately correlated noise shown in figure 2.1.B could be that of current carried across amorphous silicon films.¹⁸ In this system, charge carriers become trapped and released in an uncorrelated fashion and at a distribution of characteristic rates which is known to result in a $1/f$ spectrum. The highly correlated signal shown in figure 2.1.C could arise in a circuit with electromigration damage.¹⁹

2.4 Noise and Local Field Potentials

2.4.1 Current Theory of Local Field Potential Origin

Most researchers state that local field potentials reflect the synaptic activity of local populations of neurons. This understanding arises from a set of experiments done in the 1960s that link EEG recordings to intracranial recordings.^{2, 20-22} These studies showed that the low-frequency activity recorded in EEG is essentially independent of neuronal spiking. It was also shown that the magnitude of the fluctuations is not correlated with the properties of individual cells (as is the case for spikes), but rather they reflect the scope and geometry of the dendrites within the recording field. As discussed in the Chapter 1, cells within the cortex are arranged in layers, with the main body of neurons parallel to each other and perpendicular to the brain surface. Most people are familiar with the grooves and ridges of cortex. Within these ridges, or sulci, there are regions of relative silence where the electric dipoles created by non-parallel neurons cancel out, or at least do not sum to create the large magnitude fluctuations that are recorded in EEG.

Additional evidence for the idea that synaptic activity dominates cortical local field potentials comes from current source density experiments.²³⁻²⁵ This technique employs spatially precise electrodes to measure current sources and sinks that arise due to currents that flow across neuron membranes. It was current source density experiments that led researchers to conclude that local field potentials reflect activity over a region of approximately .5 – 3 mm from the electrode tip.²⁴

2.4.2 Gaps in the Theory

Experimental evidence suggests that synaptic activity is the primary source of fluctuations that underlie local field recordings in cortex, and suggests that no coherent oscillations could emerge in non-laminar structures, as the dipoles created by individual neurons will cancel. This is a strong prediction that makes it difficult to interpret local field potentials in non-laminar structures. In order to show that local field potentials are generated locally in non-laminar structures, researchers typically try to correlate spike activity with local field oscillations, with generally low levels of success.^{26, 27} Still, several measures suggest that oscillations can be generated within non-laminar structures.²⁸

Several researchers have discovered that processes beyond synaptic fluctuations contribute to local field potentials, yet these processes are rarely mentioned in discussions of the origin of LFPs. These processes include voltage dependent membrane oscillations and spike *after potentials*.^{4, 5} Voltage dependent membrane oscillations tend to be lower amplitude than synaptic fluctuations. After potentials have a typical duration of tens of milliseconds and have been suggested to contribute to the generation of LFP signals.²⁹

2.4.3 Potential Benefits of Noise Analysis

Section 2.2 described how different fluctuation phenomena result in different spectra and spectral characteristics. In the case of local field potentials, the different contributing fluctuations, such as synaptic potentials, voltage dependent membrane oscillations, and spike after potentials, occur on different time scales, and thus should contribute to different regions of the power spectrum. In brain regions where the cytoarchitecture is laminar, it is likely that the synaptic potentials will dominate. In structures with other cellular arrangements, the relative contribution of different mechanisms will likely depend on the unique dynamics of the local cells. Once researchers understand the noise signatures of various fluctuation mechanisms, the power spectrum could help to identify the dominant mechanisms in a particular brain structure.

While a complete theory that links microscopic fluctuations to macroscopic observables is desirable, fluctuation studies could prove useful even without that connection. Many experiments are conducted by implanting moveable electrodes which are then lowered into position over a number of days and finely tuned through the duration of a several week experiment. One inherent challenge of this experimental technique is that the researcher is essentially ‘diving blind’, only having vague information about electrode location until after the completion of the experiment. Noise spectra will likely be architecture dependent, showing differences between structures that possess different cellular arrangements. Once these differences in noise signatures are correlated with specific brain structures, researchers may be able to use this additional information to guide electrode placement during experiments.

In other physiological systems, power spectra show modulation with disease state. For example, the human heart rate tends to display a power spectrum of form $S \sim f^{-\alpha}$ with $\alpha \sim 1$ in normal adults. In subjects known to have congestive heart failure, α is typically closer to 1.5.⁹ Variations in the power spectrum of heart rate variability have also been studied in patients with diabetes and found to correlate with associated heart conditions.³⁰

The traditional ways that EEG studies are reported do not allow for conclusions regarding the modulation of power spectral slope with disease states, though they do provide enough information that one would expect to see changes. EEG is traditionally analyzed in discrete frequency bins (eg, bin theta = 4-8 Hz, bin alpha = 8-13 Hz, etc.) and many pathological states are associated with increases or decreases in power within these bins. For example, Alzheimer's disease is characterized by increased power in low frequency bands and a subsequent decrease in power within the higher frequency bands.³¹ One would thus expect to see a higher spectral slope in Alzheimer's patients relative to healthy patients. EEG is closely related to another brain recording paradigm, magnetoencephalography or MEG. Researchers studying this technique have recently learned that many pathological states show changes in the correlation of activity in different frequency ranges.^{32,33} These studies note changes in a wide range of brain diseases, including schizophrenia, alcoholism, and chronic pain. This also suggests that there will be a modulation in the power spectral slope associated with disease states.

Chapter 3

Power Spectra of Local Field Potentials

3.1 Introduction

A wide variety of disordered systems display $1/f$ -like power spectra, including noise in traffic flow⁶, fluctuations in undersea currents⁷, heart rate variability⁹, and current fluctuations in amorphous silicon films.¹⁸ Several theoretical models have been developed to account for a $1/f$ power spectrum following from underlying fluctuations. We next discuss these models and consider their potential relevance to local field potentials.

3.2 Distribution of Poisson Fluctuators

One of the more versatile frameworks for obtaining $1/f$ power spectra is that which focuses on relaxation processes within a system. At some underlying level, many systems, such as magnetic domain flipping in a ferromagnet (Barkhausen noise) and charge trapping in defects in a nanoscale semiconductor device, can be described as assemblies of fluctuators that flip between two states. This type of signal is often referred to as a random telegraph signal and a simulated example of such a signal is shown in Figure 3.1.

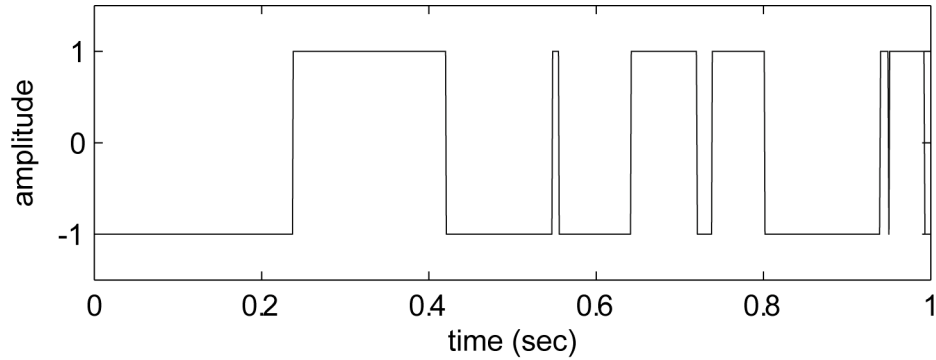


Figure 3.1 Poisson Fluctuator

A one second segment of a random telegraph type signal, or Poisson fluctuator. The lifetime of both the upstate and downstate are exponentially distributed with a characteristic time of 80 ms.

Signals of this type are also referred to as Poisson fluctuators, reflecting the fact that a key parameter of these fluctuations is described by Poisson statistics. If the distribution of times spent in each state, x , is exponentially distributed,

$$p(x) = \frac{1}{\lambda} e^{-x/\lambda} \quad (3.1)$$

then the number of transitions K between states within some time T will follow a Poisson distribution,

$$p(K) = \frac{(\mu T)^K}{K!} e^{-\mu T} . \quad (3.2)$$

The parameter, λ in the exponential distribution (3.1) is sometimes referred to as the *survival parameter* and relates to the rate parameter, μ of the Poisson distribution by

$\lambda = 1/\mu$. The distribution of lifetimes and the distribution of transitions per second for

the signal in Figure 3.1 are shown in Figure 3.2 A and B, respectively.

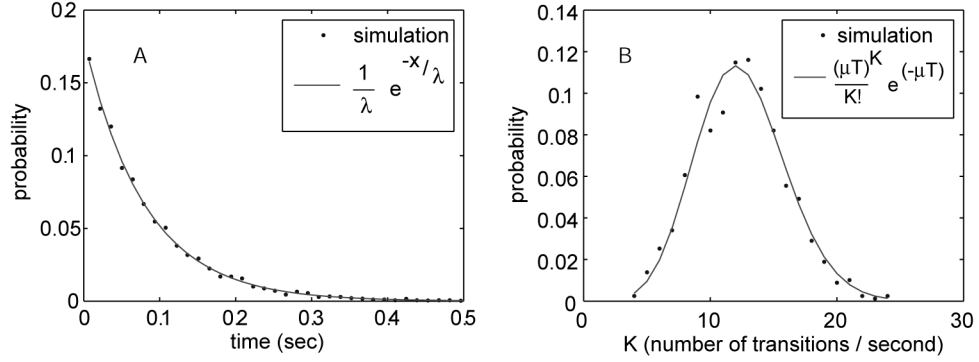


Figure 3.2 Statistical Properties of a Poisson Flucator

Distribution of lifetimes and transition rates for the signal shown in Figure 3.1. (A) The average time spend in both the up and down states is well fit by an exponential distribution, with $\lambda = 80$ ms. (B) The number of transitions per second, K , is well fit by a Poisson distribution. The distribution was calculated with a time window, T , of 1 s and μ is 12.5 flips/sec.

In these signals, the autocorrelation function is given by

$$C(t) = e^{-2\mu t} \quad (3.3)$$

and it is common to define $\tau = \frac{1}{2\mu}$, where τ can then be identified as the characteristic relaxation time of the signal. The resulting power spectrum has a Lorentzian frequency dependence,

$$S(\omega) = \frac{4\tau}{1 + (\omega\tau)^2} \quad (3.4)$$

where $\omega = 2\pi f$, and exhibits white noise at low frequencies and f^{-2} noise at high frequencies. The autocorrelation function and power spectrum for the signal shown in Figure 3.1 is shown in Figure 3.3.

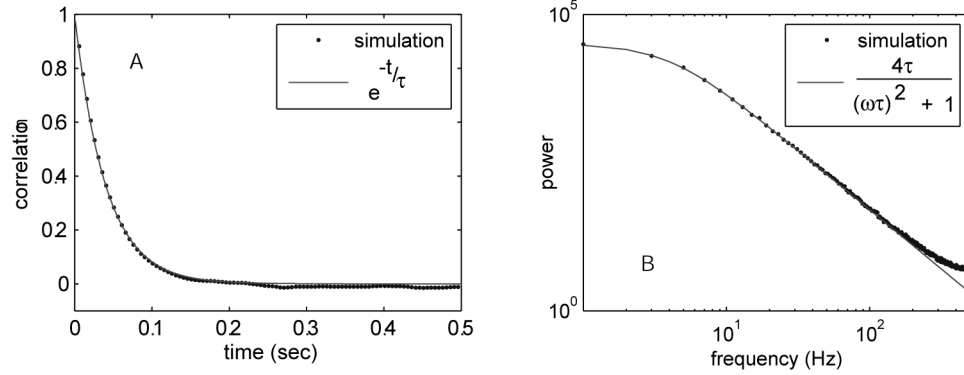


Figure 3.3 Autocorrelation and Power Spectrum of a Poisson Fluctuator
Autocorrelation function and power spectrum of the signal shown in Figure 3.1. (A) The autocorrelation function is well fit by a decaying exponential with a relaxation time, τ , of 40 ms. (B) The power spectrum is well fit by a Lorentzian, showing white noise at the lowest frequencies and f^2 at high frequencies.

Many systems possess multiple relaxation times. In these systems, the distribution of relaxation times can be written as $g(\tau)$, resulting in a power spectrum of

$$S(\omega) = \int g(\tau) \frac{4\tau}{1 + (\omega\tau)^2} \quad (3.5)$$

If $g(\tau) = 1/\tau$, then $S(f)$ will show a frequency dependence of $1/f$.

While the last constraint, $g(\tau) = 1/\tau$ is necessary to obtain a $1/f$ spectrum across all frequency and power decades, it has been found that the $1/f$ spectrum is robust against deviations from this distribution. In the case of noise in metals, it is found that the distribution is actually quite peaked and still results in a $1/f$ spectrum consistent with experimental results⁶. Experimental systems are typically only accessible across several frequency decades and non-model specific simulations show that realistic $1/f$ -like spectrum can be achieved with even a small number of independent relaxation times. Figure 3.4 shows a $1/f$ -like power spectrum over the range 1-500 Hz created with just three independent fluctuators. This simulation is not sensitive to the exact values for the

characteristic lifetime of the fluctuators. So long as there is approximately one fluctuator per temporal decade, the resulting power spectrum will be approximately $1/f$ over the corresponding frequency range.

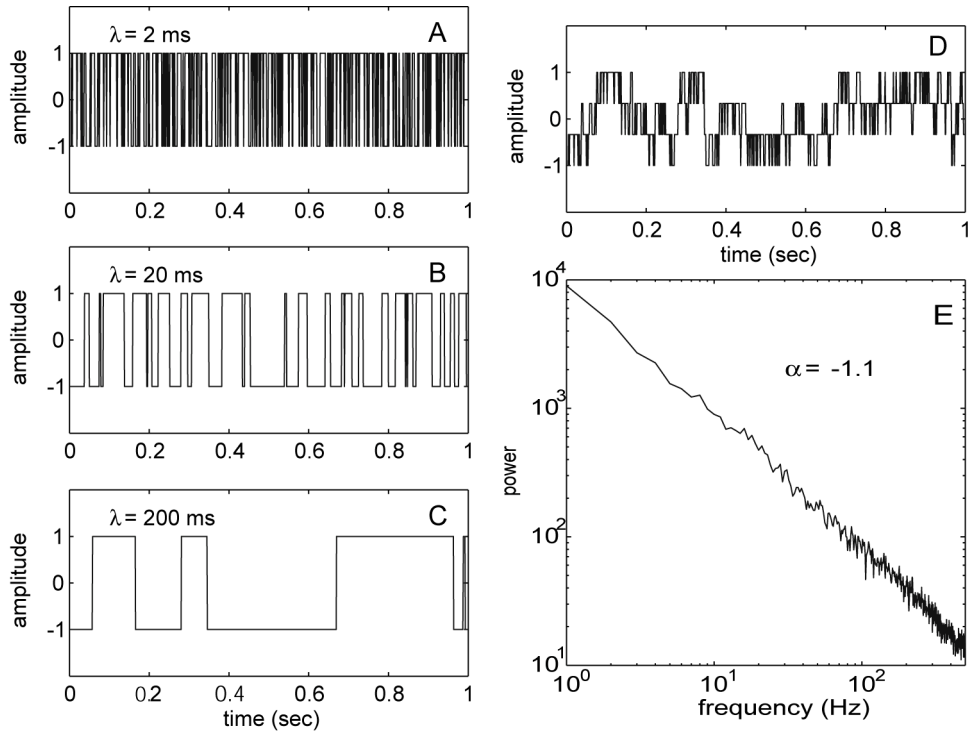


Figure 3.4 Simulation of $1/f$ Noise

$1/f$ noise can be simulated with a small number of independent Poisson fluctuators. (A), (B), and (C) One second segments of three Poisson fluctuators. (D) When the three fluctuators are added, the signal appears somewhat random. (E) The power spectrum of the signal shown in panel (D) shows a slope of -1.1 and can be considered to be $1/f$.

Local field potentials are thought to reflect electrical fluctuations occurring at synapses between neurons². These electrical fluctuations are well characterized and the times associated with them are limited in number. Some have disregarded the distribution of relaxation times model described above as irrelevant for this reason³. It is also unclear if it is relevant to consider a model that is based upon uncorrelated fluctuations. Despite

these reservations, it is premature to discard this framework as a possible explanation for the $1/f$ – like noise that is frequently observed in neural systems.

The distribution of characteristic synaptic transmission times is clearly not $g(\tau) = 1/\tau$, as there are a limited number of types of ionic channels that underlie synaptic fluctuations. Despite being limited in number, the transmission times span a significant range. The distribution of fluctuators model is based on fluctuations within a two state system. The fluctuations underlying synaptic transmission are not well modeled with such a system but instead are well represented by an α - function of the form

$$\alpha = \frac{t}{\tau} e^{-t/\tau}. \quad (3.6)$$

A simple simulation that includes physiologically relevant α -function fluctuations occurring at random, exponentially distributed times could test the relevance of this model. While nothing here can be taken as proof that the $1/f$ spectrum of local field potentials arises from a distribution of relaxation times, the argument cannot be discarded on the basis of fluctuations being physiologically limited. So long as the relevant time constants span orders of magnitudes comparable to that of the observed $1/f$ spectrum, the distribution of fluctuators model remains potentially relevant.

Synaptic alpha functions are generated by the coordinated activity of ion channels at the synapse. Individually, the activity of these ion channels resembles Poisson fluctuators.³⁴ A small segment of membrane with just one ion channel can show two conductances – one conductance when the channel is open and one when the channel is closed. It has been shown that individual channels open and close with a characteristic lifetime and exponential distribution about this lifetime.^{35, 36} These channels show

characteristic Lorentzian power spectra. As discussed and shown in figure 3.4, a spread of characteristic lifetimes would result in $1/f$ noise, if the activity of the channels was independent. Despite the fact that channel activity tends to be highly correlated, this could suggest that the activity of the individual channels plays a larger role in local field potentials than previously thought.

3.3 Frequency Filtering Properties of Dielectric Media

In the simple situation of a voltage recorded across a resistor, fluctuations in the voltage can occur due to thermal fluctuations within the resistor. The resulting power spectrum, termed Johnson noise, is frequency independent and given by

$$S_v(f) = 4kTR. \quad (3.7)$$

If instead of an ideal resistor, we consider the noise arising within a dielectric material, we can write

$$S_v(f) = 4kT \operatorname{Re}(Z) \quad (3.8)$$

where $\operatorname{Re}(Z)$ is the real part of the system's impedance. In an ideal capacitor, the real impedance is zero. Any actual capacitor has some real resistive impedance and the actual capacitor can be modeled as a parallel system of an ideal parallel plate capacitor and a resistor. For this system, the impedance is given by

$$Z = \frac{R}{1 + (R\omega C)^2} - i \frac{R^2 \omega C}{1 + (R\omega C)^2} \quad (3.9)$$

resulting in a voltage noise spectrum of

$$S_v(f) = 4kT \frac{R}{1 + (R\omega C)^2} \quad (3.10)$$

where R is the parallel resistance and C the ideal capacitance of plate area A and plate spacing d .

An ideal capacitor is characterized by a purely real dielectric constant with no energy dissipated as heat. In reality, all dielectric materials possess a complex dielectric constant typically denoted by

$$\epsilon_r(\omega) = \epsilon_r'(\omega) + i\epsilon_r''(\omega). \quad (3.11)$$

The real component, ϵ_r' , represents the relative permittivity as used to calculate capacitance, as in

$$C = \frac{\epsilon_r' \epsilon_0 A}{d} \quad (3.12)$$

The imaginary component relates to the materials conductivity and accounts for the energy dissipation that occurs through polarization and relaxation processes.

By considering the admittance, the reciprocal of impedance, of both the real and modeled systems, the ideal model parameters (C_{ideal} and R) can be related to the measurable dielectric constants. For the real system,

$$Y = i\omega C_{real} = i\omega \frac{\epsilon_0 A}{d} \epsilon_r(\omega) = -i\omega \frac{\epsilon_r' \epsilon_0 A}{d} + \omega \frac{\epsilon_r'' \epsilon_0 A}{d} \quad (3.13)$$

while for the modeled system,

$$Y = \frac{1}{Z} = -i\omega C_{ideal} + \frac{1}{R} \quad (3.14)$$

Thus, the ideal model parameters are given by

$$C_{ideal} = \frac{\epsilon_r' \epsilon_0 A}{d} \quad \text{and} \quad R = \frac{d}{\omega \epsilon_r'' \epsilon_0 A}. \quad (3.15)$$

Substituting these parameters into equation 3.10, defining the loss tangent as

$$\tan(\delta) = \frac{\epsilon''}{\epsilon'} \quad (3.16)$$

and considering the limit where $\epsilon'' \ll \epsilon'$ results in a power spectrum of the form

$$S = 4kT \frac{1}{\omega C} \tan(\delta) \quad (3.17)$$

For dielectric materials with a frequency independent loss tangent, the power spectrum resulting from random thermal fluctuations will show a $1/f$ frequency dependence. A wide variety of solid dielectrics and many liquid dielectrics possess this property with nearly frequency independent loss tangents over the range of 10^{-2} Hz through 10^8 Hz.³⁷

The loss tangent of brain tissue has not been explicitly studied, though there have been studies of dielectric properties of biological tissues that may help to test the relevance of this model³⁸⁻⁴⁰. In these studies, researchers used three different techniques to measure the permittivity and conductivity of harvested brain tissue over the range of 10 Hz to 20 GHz.

There are several reasons to question the applicability of these experiments. The tissue used in that experiment was from recently euthanized animals with measurements made several hours after death. Older work has shown that cerebral impedance changes abruptly and significantly within minutes after circulatory arrest⁴¹. Using deeply anesthetized and intact animals, measurements could be obtained in hemodynamically normal animals with normal boundary conditions provided by the intact skull. The particular probes used required a large piece of brain tissue – significantly larger than that available from rats and, more importantly, significantly larger than the heterogeneities within brain tissue. Ideally, the impedance measurements

would be made with the same probes used in recording the local field potential samples in order to equally account for the potentially unknown frequency dependencies of the probe impedance.

This section outlined an approach to interpreting the power spectral slope by considering the structural properties of brain tissue as characterized by the dielectric loss tangent. In the case of brain tissue, the loss tangent is likely heavily influenced by electrostatic effects at the interface of the extracellular space and the cell membrane. The same properties that influence the loss tangent will also influence diffusion of molecules throughout the extracellular space. These properties include complex neuronal morphologies, the presence of large biological macromolecules and cellular swelling, among others. While the dielectric properties of brain tissue have not been explicitly studied, other structural parameters related to diffusion have been investigated by researchers interested in the diffusion of neuroactive substances.⁴² One of these parameters is the extracellular space volume fraction, denoted *alpha*, and defined as the ratio between the volume of the extracellular space and the total volume of tissue. In the adult brain, the volume fraction is roughly 20% with variations between brain structures.

Many pathological states exhibit changes in the diffusion properties of extracellular space.^{43, 44} Researchers have measured significant changes in model systems of epilepsy⁴⁵, Parkinson's disease⁴⁶, and Alzheimer's disease⁴⁷, among many others. It would be interesting to study the local field potentials in the disease model systems used to study diffusion parameters. If the composition of the extracellular space plays a

significant role in the frequency properties of local field potentials, one would expect to see a difference in the power spectra recorded from normal and pathological systems.

It should be noted that the two previously discussed models of $1/f$ noise are likely mathematically identical despite the different formalism and physical considerations in their derivations. While I discussed the macroscopic properties of a leaky dielectric medium, one could also consider the microscopic behavior of such a system. In the presence of an electric field, molecules within the material become polarized. Upon removal of the field, random collisions reduce the induced dipole moment over some characteristic time. Given the extreme molecular heterogeneity of the brain, it is reasonable to expect a wide distribution of dipole relaxation times. While the first situation considered opening and closing ion channels as the origin of the fluctuations, the second situation considers the source to be molecular alignment and relaxation.

3.4 Self-Organized Criticality

Self-organized criticality is a framework that was proposed by Bak, Tang, and Weisenfeld in 1987 to describe the behavior of complex dynamical systems.⁴⁸ Their hypothesis was that systems organize themselves into a complex state that lacks any characteristic spatial or temporal scale. This suggestion combined two concepts familiar to many neuroscience researchers – self-organization and critical behavior. They report that $1/f$ noise arises from the dynamics of these self-evolved critical states. There are several indications that self-organized criticality could be applicable to neural dynamics, including $1/f$ frequency scaling. It is necessary to critically examine this idea from both a theoretical and experimental perspective before any definite statements can be made

regarding the relevance of self-organized criticality to any particular dynamic neural signal.

In order to test the hypothesis that self-organized criticality can explain the $1/f$ noise observed in local field potentials, it is first necessary to carefully examine both what self-organized criticality is and what it is not. As described by Bak, Tang and Wiesenfeld, as well as by the many researchers that have explored this idea, self-organized criticality is a framework through which models for specific systems can be developed. It is not a model in and of itself. There is no concise definition of self-organized criticality, but rather there are a number of characteristics displayed by candidate systems. These include ⁴⁹:

- The system's behavior arises due to many interacting degrees of freedom
- The system's behavior is dominated by mutual interactions of many degrees of freedom
- The system evolves to a critical, metastable state with no outside tuning
- The system's critical, metastable threshold can be reached through a large number of microscopic configurations
- The system operates under a slow drive such that the system can relax from one metastable state to another
- The statistical properties of the system are described by power laws

Researchers in many disparate fields have constructed models based on the characteristics of self-organized criticality. The most frequently noted examples are those of sand piles, earthquakes, and forest fires, but models have also been developed for

economic systems and biological evolution. In all of these cases, the resulting model is very system specific; there is no mathematical formalism that can be mapped onto different systems. In order to develop a self-organized criticality based model for local field potentials, one would need to start with the underlying fluctuations and try to apply the above listed characteristics.

Self-organized criticality can also be tested experimentally. A system possessing the characteristics of self-organized criticality will show fluctuations due to driven dynamics rather than equilibrium fluctuations. The nature of the fluctuations can be analyzed through higher order statistics.^{50, 51} Self-organized criticality requires that events at one temporal scale set the stage for events on another scale. This flow of activity from one scale to another can be captured in higher order correlation functions. These analytical methods are particularly susceptible to extraneous noise sources, thus extra care must be taken to ensure that the recorded signal is uncontaminated. This could be particularly challenging in living systems and it may be best to first test this theory in prepared slices.

As emphasized in Chapter 1, there are different signals that can be recorded from neurological systems and they reflect different underlying physiological fluctuations. Even if researchers find that self-organized criticality can account for a certain neurological signal, it should not be concluded that ‘the brain’ shows self-organized criticality until we have a better understanding of how the various neurological signals relate to each other. None of these observations and constraints should be interpreted to mean that self-organized criticality does not describe some aspect of neural dynamics, but

rather that much work must be done before one could claim that this paradigm is applicable.

Chapter 4

Experimental Methods

Data for the analyses presented in Chapters 5 and 6 was originally collected for a variety of rodent navigation experiments. Hippocampal data was collected by Jadin Jackson and Chris Boldt.^{52, 53} Striatal data was collected by Neil Schmitzer-Torbert,^{54, 55} and the postsubicular data was collected by Kelsey Seeland and Adam Johnson.⁵⁶

4.1 Brain Structures

4.1.1 Hippocampus

The hippocampus is a well-studied brain structure involved with learning and memory (see reviews by O'Keefe and Nadel¹², and Redish⁵⁷). In rodents, the hippocampus is noted for having cells that are only active when the animal is in a particular region of its environment. The local field potentials generated in the hippocampus are also well characterized. Oscillations that occur at 6-10 Hz are labeled 'theta' oscillations and persist for up to minutes, when the animal is engaged in attentive behaviors.^{12, 13} During periods of rest and autonomous behaviors, this strong 6-10 Hz oscillation is not present and the activity is largely irregular, even being referred to as Large Irregular Activity (LIA). These epochs of LIA are punctuated by 160-200 Hz oscillations known as sharp waves. Sharp waves are characterized by ripples at the given frequency with a characteristic duration of 100 ms.¹⁴ Past work on hippocampus has revealed significant aspects of hippocampal dynamics by investigating the interplay of cellular spike activity with these LFP states. The hippocampus provides an ideal structure

in which to study local field potentials due to the laminar structure and the strong interaction between cellular spike activity and LFP oscillations.

4.1.2 Postsubiculum

The postsubiculum is another brain structure involved in navigation. It is a cortical structure that is closely interconnected with the hippocampus and its cellular architecture is layered just as in visual and motor cortex. Head direction cells were first identified in this structure.⁵⁸ These are cells that show peak firing activity when the animal is facing a particular direction and their firing decreases monotonically as the orientation deviates from that preferred direction.⁵⁹ This spatial tuning, along with anatomical connections with other structures thought to be involved with navigation make the postsubiculum an interesting experimental target. From the perspective of local field potentials, postsubiculum is interesting because of its laminar structure and the potential relevance to EEG, which is thought to reflect cortical synaptic activity.

4.1.3 Striatum

The striatum is a subcortical structure that, compared with hippocampus and postsubiculum, is relatively unexplored. Classically, this structure has been considered a motor structure and has been studied with regards to the role it plays in several major diseases. Local field potentials have only recently begun to be characterized and studies show oscillations in different frequency ranges. Low frequency oscillations (~ 8 Hz) and gamma oscillations (~30–80 Hz) have been recorded from rats,²⁶ and beta oscillations (10-30 Hz) have been recorded from monkey striatum.⁶⁰ Work done by Schmitzer-Torbert and Redish, through experiments for which the data studied here was collected,

found cellular firing correlates such as spatial location and reward-delivery.^{55, 61} Striatum is a non-laminar structure, and thus recording from this structure could provide data useful for deciphering the origin of LFP oscillations in structures that lack regular cellular arrangements.

4.2 Animals

All animals used were Brown-Norway Fisher-344 Hybrid rats (BNF1) and were aged 7-18 months at the time of recording. Animals were food-restricted during behavioral training and testing. All procedures were approved by the IACUC at the University of Minnesota and were in accordance with NIH guidelines for animal care.

4.3 Behavioral Tasks

The data in this study came from rats trained on a number of different behavioral tasks. Sessions ran from 20 to 40 min, depending on the specifics of the task. The hippocampal data was taken from rats performing the Linear Track task⁶², and Open Field Goal task.⁶³ The postsubicular data came from rats performing the Open Field task.^{64, 65} The dorsal striatal data came from rats performing the Multiple-T task⁶⁶ and NosePoke task.⁶⁷

In the Linear Track task shown in Fig. 4.1, rats ran back and forth on a 1.25 m linear track, receiving food at both ends. Pellets were delivered upon entry into a goal region near the feeder and the region was not re-armed until the animal triggered the goal zone at the opposite end of the track.

In the Open Field task (Fig. 4.2), animals foraged for food in a 1m diameter cylinder with a cue-card subtending 90 degrees. The cue-card provides a navigational

landmark. Food was delivered randomly with a Poisson interval ($\lambda = 10$ s). In the Open Field Goal task, rats also foraged for food in the 1 m cylinder, but food was only delivered when rats crossed a 7 cm diameter goal region. The goal was re-armed only after rats had been outside of a 14 cm diameter region around the goal for 4 s. The goal zone was invisible and the location varied from session to session.



Figure 4.1 Linear Track Task

The Linear Track task schematic. Animals ran back and forth on the track to trigger food reward upon entry to a goal region near each feeder. The goal zone was not re-armed until the animal triggered the goal zone at the opposite end of the track.

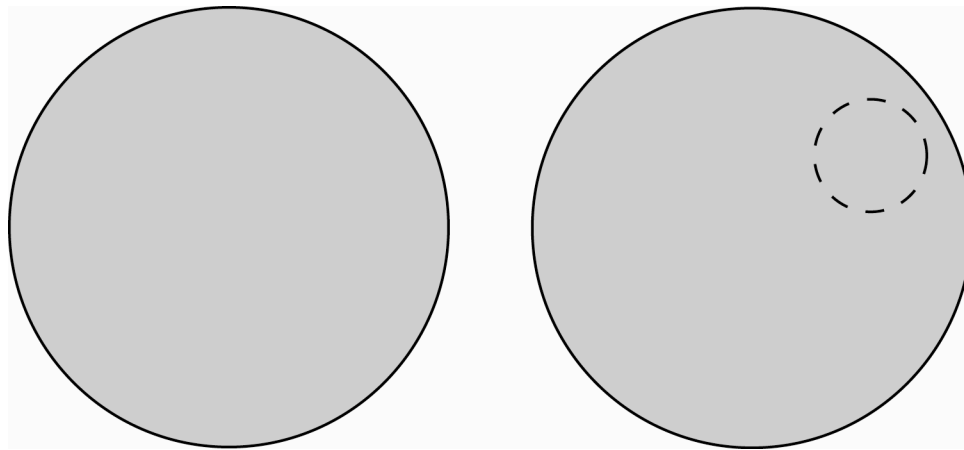


Figure 4.2 Open Field and Open Field Goal Tasks

Schematic of the Open Field and Open Field Goal Tasks. *Left* In the Open Field task, animals foraged for food pellets that were delivered randomly. *Right* In the Open Field Goal task, animals needed to locate the goal region to trigger food delivery.

In the NosePoke task, shown in Fig. 4.3, a rat had to hold his nose in a nose-poke port in order to break an LED beam. If the LED beam was interrupted for 500 ms, food became available at the other end of the 1.25 m track. The beam was not re-armed until the rat had traveled to the other end of the track and received its food.

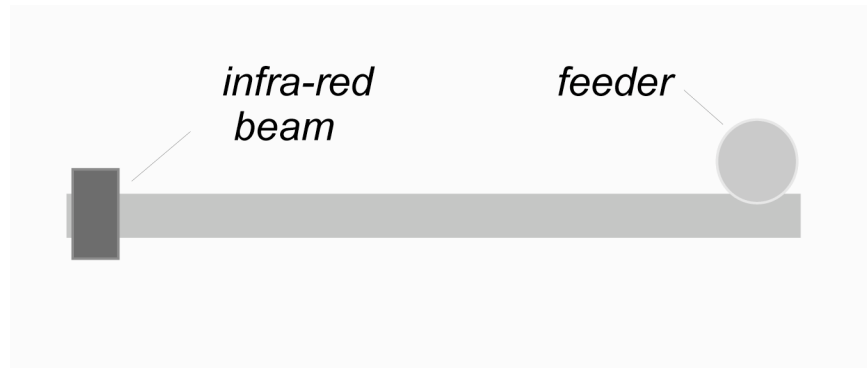


Figure 4.3 Nose Poke Task

The Nosepoke task schematic. A nosepoke port and a pellet dispenser were placed at opposite ends of a linear track. Rats were required to interrupt the infrared beam in the noseport port for 100 ms in order to activate the pellet dispenser.

In the Multiple-T task, rats ran through a sequence of four T-choices in order to receive food. The last choice led to a return path, so the task entailed running a 4 m loop for food (see Figure 4.4). Food was provided at two sites on each return rail. On any specific day, only one pair of sites (i.e. the right or left return rail) was active and provided food reward. The other pair of feeders remained in their usual positions on the track, but did not provide reward. The sequence of choices remained constant within a day, but changed between days. Rats were allowed to run for one 40 minute session daily.

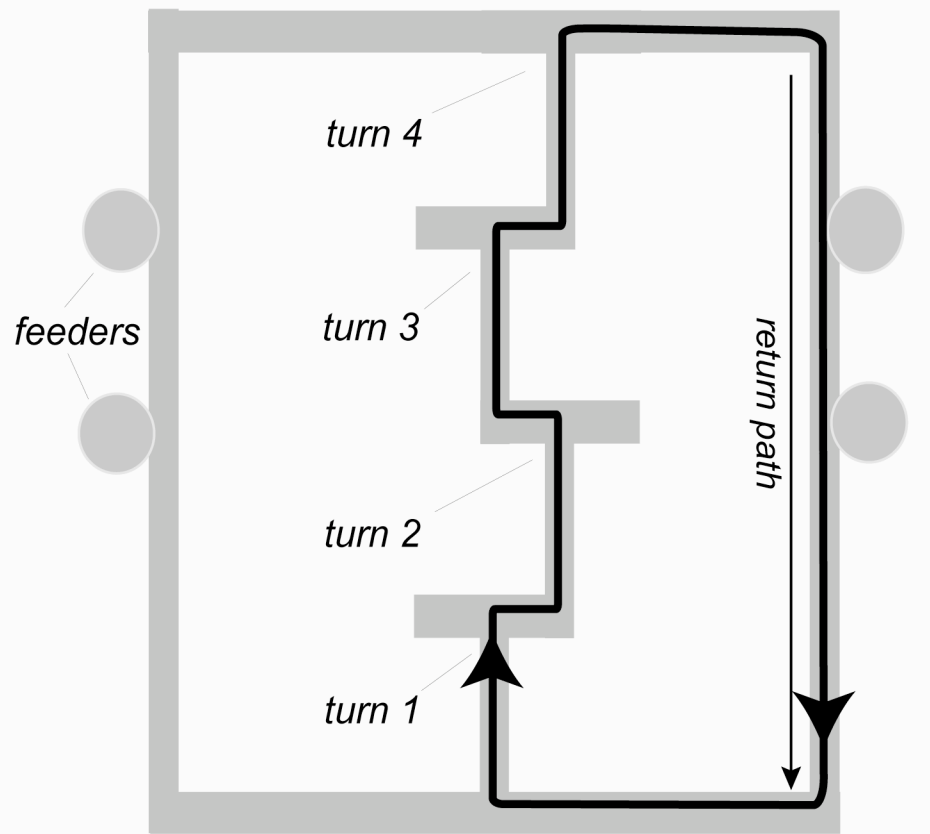


Figure 4.4 Multiple-T Task

Schematic of the Multiple T maze. The path of the animal is indicated by the dark line. The four filled circles indicate the locations of the feeders on the *return rails*. Each day, the *turn sequence* (which in this case was right-left-right-right) remained constant, but between days the turn sequence could be changed. On each day, only one pair of feeders was active (either the left or the right pair of feeders), providing a fourth choice to the turn sequence. The animal ran a continuous one-way loop, receiving food at the correct feeders on each trial.

In the Take-5 task, four feeders were placed around a rectangular track (90 cm x 60 cm), one feeder at the center of each side. In order to receive food, rats had to run $5/4$ around the track in a clockwise direction (see Figure 4.5). Thus if a rat received food at the west feeder, the rat had to make one full circuit around the track, returning to the west

feeder, and then continue on to the north feeder in order to receive food. Rats were allowed to run for one 40 minute session daily.

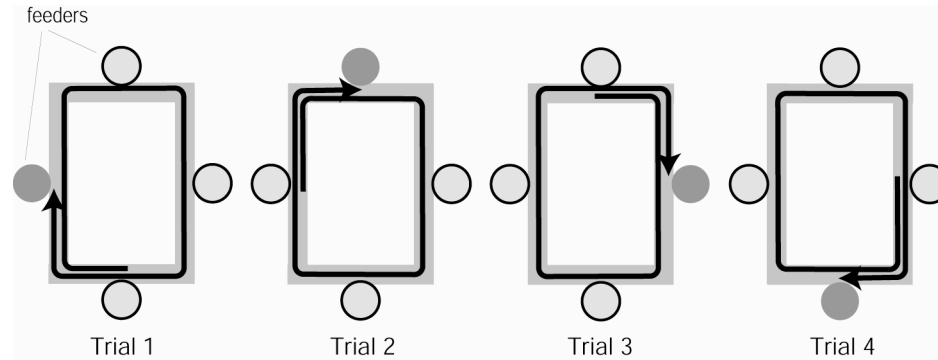


Figure 4.5 Take-5 Task

Rats ran on a rectangular track for food which could be delivered to any side of the track. In each trial, rats were required to run 1.25 times around the track. Illustrated are four successive trials, in which the rat first received food reward on the west side of the track, then subsequently received food on the north side of the track. The path of the rat in each trial is shown by the black arrow, and the rewarded feeder in each trial is shaded dark.

4.4 Neural Recording

Local field potentials were recorded from one channel of a four channel tetrode, shown schematically in Fig. 4.6. The four wire tetrode is useful for providing source separation for extracellularly recorded action potentials (spikes). Tetrodes allow the researcher to discriminate spikes from multiple neurons, by comparing the spike waveform properties across channels. The recorded voltage trace depends on the spatial relationship between the neuron and the four tetrode channels and the differences in waveform properties can be exploited to separate spikes arising from different neurons. Local field potentials reflect the electrical activity over a distance much larger than the

separation of electrode tips, and thus the signal is nearly identical between the four recording sites. For all analyses, only one channel of each electrode is considered.

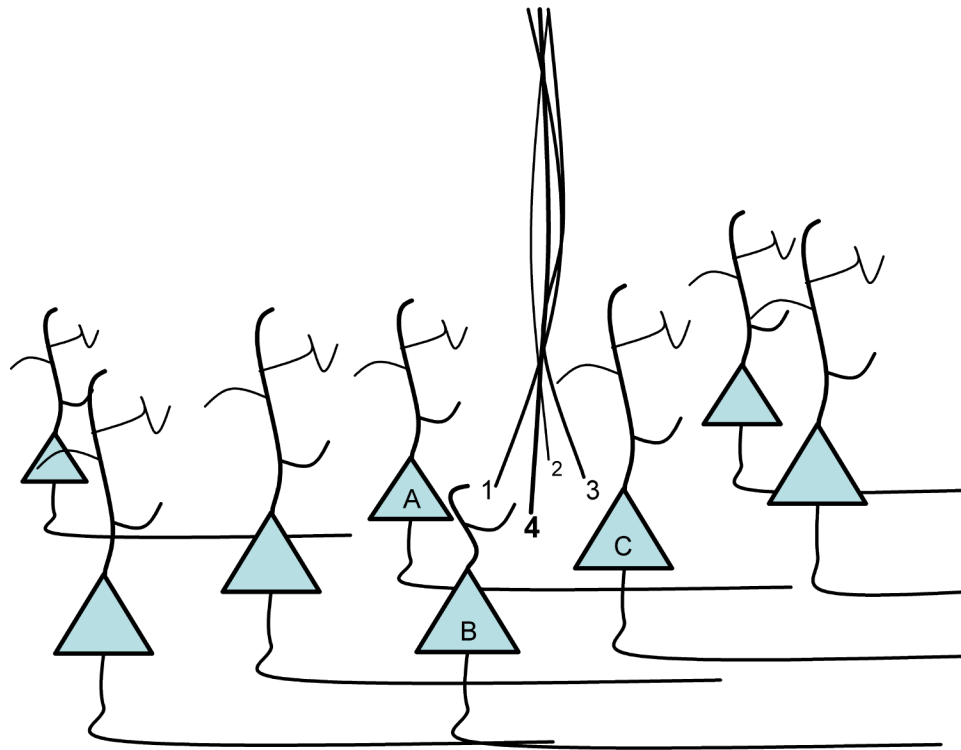


Figure 4.6 Tetrode Schematic

The tetrode is depicted as 4 black strands intertwined. Voltage traces arising from spikes (high frequency activity) from neuron A will be larger on channel 1 than on channels 2 and 4, and much larger than channel 3. Local field potentials reflect activity from a larger area, and thus the LFP signal recorded from each channel is nearly identical. Figure courtesy of Jadin Jackson.

LFPs were recorded with 16 channels of a Cheetah 64-Channel system (Neuralynx, Tucson AZ). A 72-channel torque-sensing, motorized commutator (AirFlyte, Bayonne, NJ; Dragonfly, Ridgeley WV; Neuralynx, Tucson AZ) allowed the animals to run without twisting the shielded cables connecting the electrodes to the recording system. Signals were amplified at unity-gain at a headstage (Neuralynx) directly connected to the implant, passed along the cables and commutator before reaching two

variable gain (1-50,000x) Lynx-8 amplifiers (Neuralynx). Amplification was typically 500x though this was variable and automatically recorded into each data file. The signals were passed through a Cheetah A2D processor and stored at a sampling frequency of 943 or 2003 Hz. All local field potential signals were filtered at 1-475 Hz in the amplifiers.

4.5 Surgery

Tetrodes were made from 14 micron NiChrome wire (Kanthal Precision Wire, Palm Coast, FL). Tetrodes were loaded into hyperdrives (David Kopf Instruments, Tujunga, CA), providing individual microdrives for each of 12 tetrodes and 2 single-wire electrodes used as references for common noise rejection. Hyperdrives were implanted stereotactically over the target location (hippocampus: Bregma -3.8 mm AP, +2.0 mm ML; postsubiculum: Bregma -7.0 mm AP, +2.4 mm ML; dorsal striatum: Bregma +0.5 mm AP, 3.0 mm ML). Surgery was done under general anesthesia (sodium pentobarbital 40-50 mg/kg, maintained with isoflurane 0.5-2%, vaporized into pure oxygen, delivered at 1.0 L/min) and under sterile conditions. Signals from the tetrodes were measured relative to a ground screw implanted during surgery in the parietal bone. After surgery, electrodes were lowered into place over the subsequent 1-3 weeks.

4.6 Position and Velocity

For all experiments, position was sampled at 60Hz via a camera in the ceiling tracking LEDs on the headstage of the animal (Cheetah, Neuralynx). Video data was timestamped synchronously with the electrophysiological data and pixels that broke manually determined thresholds were recorded to disk. The video data was accessed in

real-time to facilitate automated behavioral controls, such as delivering food pellets in response to specified behaviors.

A linear speed could be calculated for the LinearTrack and NosePoke tasks. For the Multiple-T and Take-5 tasks, the overall motion was essentially angular around a skewed circle. Thus, only the angular components around the pseudo-center of the track were included in the speed calculations. Speed was calculated using the adaptive windowing procedure described by Janabi-Sharifi et al.⁶⁸ This algorithm provides for both accurate speed estimates and an accurate estimate of the time of speed change. Speed estimates received from this algorithm were subsequently smoothed with a 300 ms Hamming window.

Chapter 5

Analytical Technique

5.1 Introduction

Standard techniques for identifying fundamental frequencies typically entail applying a fast Fourier transform (FFT) to the time-series and then examining either the power spectrum or the spectrogram. The power spectrum assumes that the data are stationary in time, an assumption that is invalid for almost all neural data. Non-stationary oscillations are difficult to identify within an average power spectrum because the characteristic frequency peak only occurs in a limited number of time-windows. Averaging across time-windows dilutes the magnitude of the characteristic peak so that it may be difficult to resolve from background fluctuations. The spectrogram does not assume stationarity, in that it measures the power at each frequency as a function of time, but examining a spectrogram for a long data session is extremely difficult because each time-window contributes only one column to the spectrogram. Since neural data tend to have a low signal-to-noise ratio, identifying the fundamental frequencies within each time-window can be difficult.

5.2 Overview of Technique

Instead of averaging the separate samples of the spectrogram, we propose correlating the power values at each frequency across the time-samples within the spectrogram. For Gaussian processes, the two-point autocorrelation function contains all the relevant information concerning the physical mechanisms underlying the fluctuating

time series^{6, 69}, as the magnitude of the FFT amplitudes at one frequency are uncorrelated with the FFT amplitudes at another frequency⁷⁰. However, interactions between fluctuators can produce significant time-dependent variations in the power spectra with non-trivial correlations. These can be quantified through the calculation of a conventional correlation coefficient ρ_{ij} , where the indices i and j denote differing frequencies within the same time-series. Since any characteristic oscillation arising from a biological rhythm will have a finite, non-zero width, it will overlap with adjacent frequencies, and thus will show a non-zero correlation with these neighboring frequencies, even if it does not interact with other oscillations.

5.3 Analysis Methods

The time-dependent fluctuations of the voltages $V(t)$ recorded from the tetrodes were first broken into individual continuous, contiguous, non-overlapping time-windows. The extent of the time-window determined the lowest frequency in the Fourier transform of $V(t)$, while the data acquisition rate constrained the upper frequency. The voltage was fast Fourier transformed and then multiplied by its complex conjugate, to yield the spectral density as a function of frequency.

The correlation between the power spectrum $S(f)$ at a frequency f_i and at another frequency f_j can be calculated using the expression

$$\rho_{ij} = \frac{\sum_k (S_k(f_i) - \langle S(f_i) \rangle)(S_k(f_j) - \langle S(f_j) \rangle)}{\sigma_i \sigma_j} \quad (5.1)$$

where $S_k(f_i)$ is the spectral density at frequency f_i in time-window k , $\langle S(f_i) \rangle$ the average spectral density magnitude at frequency f_i , σ_i is the standard deviation of $S(f_i)$, and k

ranges over the total number of time-windows. Because the spectral density at any frequency will always be perfectly correlated with itself, ρ_{ii} will always be unity. Time-windows in which the recorded voltage exceeded the maximum range of the analog-to-digital converter were removed from analysis.

These correlations can be visualized through standard correlation plots (for example, Fig. 5.2 and Fig. 5.3). In these figures, correlation coefficient values of zero are shown as dark while high correlations are in white. No significant anti-correlations ($\rho_{ij} < 0$) were found. In these plots, the diagonal represents ρ_{ii} and thus has a value of 1 by definition. Since $\rho_{ij} = \rho_{ji}$, the upper triangles of these plots are redundant with the corresponding lower triangles, but have been included for convenience. Biologically-generated fundamental frequencies appear as areas of high correlation and are reflected by symmetric grey regions near the diagonal. Off-axis dark regions indicated interactions between oscillators. Non-biological signals (such as 60 Hz electrical background noise) appear as sharp, uncorrelated lines in these plots.

5.4 Results

This simple methodology provides a novel means of determining the fundamental oscillation frequencies within a neural structure. In Sections 5.4.1 – 5.4.3 we first test this method with simulations, inserting known fluctuators into an example recording. We then show that in hippocampus, in which characteristic LFP oscillation frequencies are well known, this method identifies the known frequencies. We then apply the method to a new aspect of a structure with known oscillations (postsubiculum, part of cortex).

Postsubiculum showed oscillation components similar to other aspects of cortex. Finally,

we apply the method to the dorsal striatum, where the fundamental LFP oscillation frequencies are unknown, and identify novel oscillatory components there.

5.4.1 Simulation

In order to test the capabilities of the method proposed here, simulations were used to create a time-series in which all oscillation frequencies were known. Applying the method to these simulations indicated that fundamental oscillations can be detected through the correlation coefficient analysis even while remaining undetected using standard frequency analysis techniques.

For this simulation, a voltage time-series from a single tetrode channel was recorded from an animal performing the NosePoke task. The single voltage time-series from the single tetrode channel that was analyzed exhibited primarily Gaussian $1/f$ noise (Fig 5.1.A). A spectral density is considered Gaussian if it arises from a large number of statistically independent fluctuators, so that the magnitude of the spectral density at one frequency is uncorrelated with the power spectrum at a differing frequency. In the power spectrum (Fig. 5.1.C), external electrical noise was observed as sharp peaks at 60 Hz and the odd harmonics. The spectrogram (Fig. 5.1.E) contains essentially the same information. The correlation matrix (Fig. 5.1.G) shows that most power correlations are equal to zero. One can faintly see the absolute zero correlation of the 180 Hz noise harmonic.

Oscillations were then added to the signal. The oscillations were sine waves of various frequencies, all with amplitude equal to the rms value of the original voltage signal. One of the oscillations was comprised of a 100 ms 50Hz oscillation followed

immediately by a 75 ms 100Hz oscillation. The original signal was divided into 1 second segments and this oscillation was placed into 10% of the segments, selected randomly. The second oscillation was simply a 50 ms, 150 Hz oscillation that was placed into 10% of the time segments, also selected randomly.

The power spectrum of the modified signal (Fig. 5.1.D) shows the increased power over the designated frequencies but the change is small enough to be difficult to distinguish from other bumps in the spectrum. The oscillations are not visible in the spectrogram (Fig. 5.1.F) demonstrating that an oscillation that occurs completely within one time slice will not be visible given the large number of time slices examined. Finally, the correlation matrix (Fig. 5.1.H) was computed, which unambiguously displays the structure that was placed in the signal. One can clearly see both the frequency of each oscillation in the high correlation regions centered on the diagonal, as well as the inter-oscillator correlations shown by the region of high correlation off the center axis.

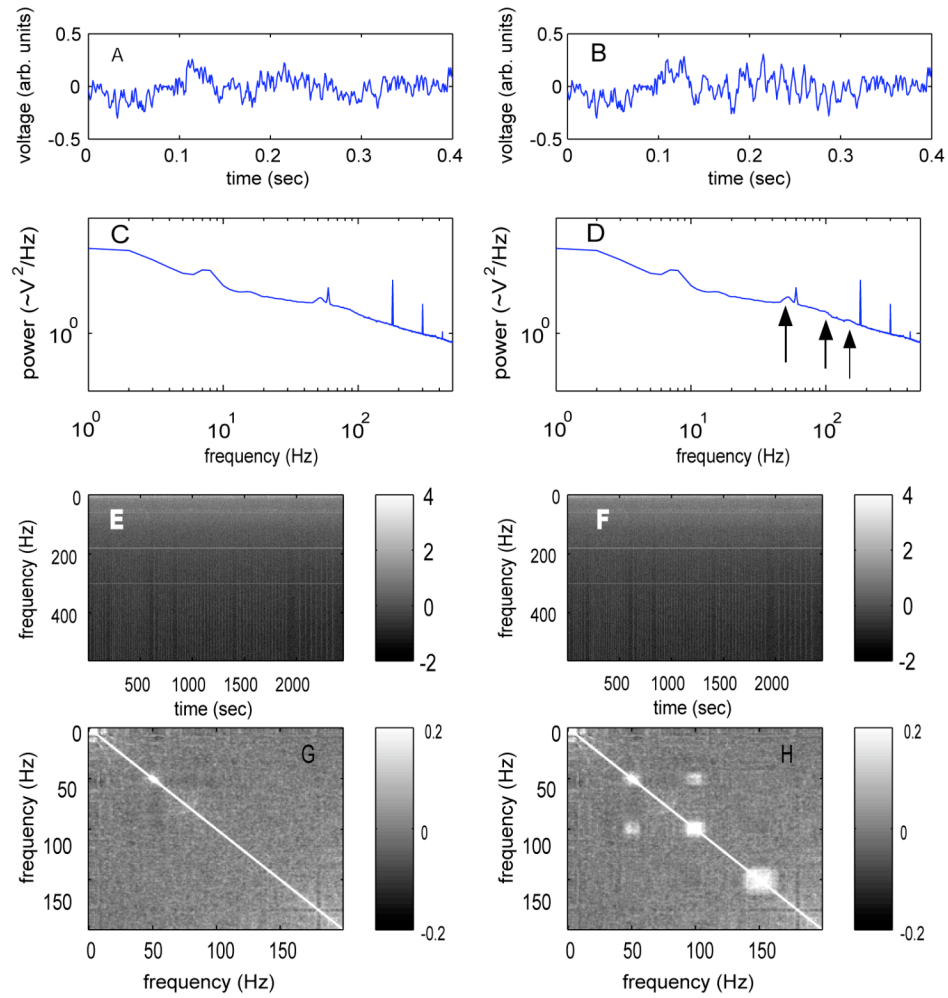


Figure 5.1 Simulation

Simulation showing how the correlation method can identify the occurrence of coherent oscillations within a noisy signal. (A) and (B) Time series of the original and modified signal, respectively. (B) includes a 100 ms 50Hz oscillation followed immediately by a 75 ms 100 Hz oscillation. (C) and (D) Power spectra of the original and modified signals. The arrows in (D) point to the small increases in power associated with the added oscillations. (E) and (F) Spectrograms of the original and modified signals. Because the oscillations were added intermittently, they are nearly invisible in the spectrogram. (G) and (H) Correlation plots of the power spectra of the signals show in (A) and (B). The uniform zero correlations in (G) show that the original signal consisted of Gaussian fluctuators with no fundamental frequencies. Three fundamental frequencies are clear in (H) and correspond to the frequencies indicated by the arrows in (D). The diagonal in panels (G) and (H) represents the correlation of each frequency with itself and thus has a value of 1 by definition.

5.4.2 Hippocampus

Local field potentials recorded from the CA1 region of the hippocampus show two major oscillatory frequencies, characterized as theta (7-14 Hz), which occurs during awake, attentive and REM states^{12,13}, and ripples (200 Hz)¹⁴, which ride on sharp-waves that occur during slow-wave-sleep and inattentive states.⁷¹ Other oscillations can also be seen in hippocampal structures (such as gamma oscillations; 50-100 Hz)⁷², but these do not show strong power in CA1 stratum pyramidale.⁷³ In order to test the capabilities of our proposed method to identify fluctuators in real situations, we measured local field potentials from tetrodes chronically implanted in the dorsal hippocampal pyramidal layer.

As can be seen in Fig. 5.2, there were clear regions of high activity in the low frequency range (0-20 Hz) and in a high-frequency range (160-220 Hz). Examination of the low-frequency range finds a strong fluctuator at 5-15 Hz, likely to be the theta signal. The very sharp, uncorrelated 10 Hz signal slicing through the correlation coefficient plot is non-biological; it was generated by the firing of the automated pellet-delivery feeders. The high-frequency power block is likely to have arisen from ripples which typically show oscillations in the range of 140-200 Hz.^{14, 74}

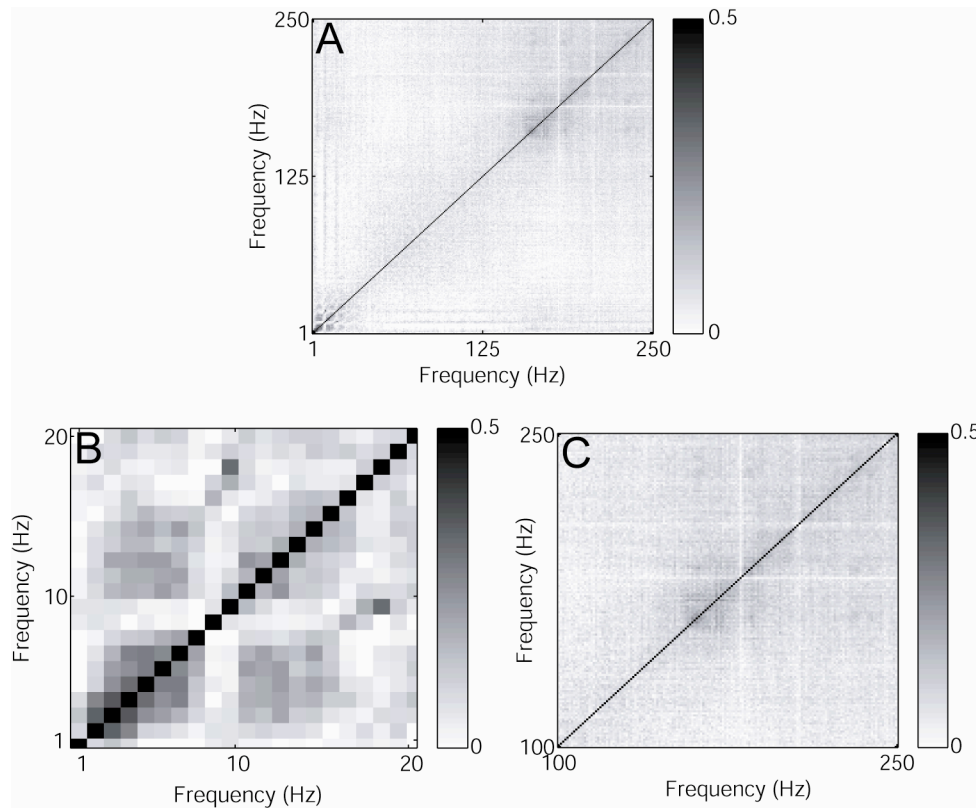


Figure 5.2 Correlation Structure of LFPs Recorded from the Hippocampus of Two Rats

(A) Correlation matrix of all frequencies ranging from 1 to 250 Hz. Note the clear blocks in the low frequency (0–20 Hz) and high-frequency (160–220 Hz) ranges. (B) Expanded plot of the correlation matrix of the frequencies ranging from 1 to 20 Hz. Note the strong 5–15 Hz oscillator (theta). The uncorrelated 10 Hz oscillator (with its 20 Hz harmonic) is non-biological; it is generated by the firing of automated pellet delivery feeders during the behavioral task. (C) Expanded plot of the correlation matrix ranging from 100 to 250 Hz. Note the 160–220 Hz component. Figure from Masimore et al, 2004.

5.4.3 Postsubiculum (cortex)

The local field potential oscillation structure of hippocampus is well known, and our method found the key frequencies previously identified. We next apply the method to a structure where the specific frequencies are not known, but can be inferred from similar structures.

Fundamental oscillatory frequencies have been well-studied in cortex, particularly through extracranial EEG⁷⁵ and in local field potentials recorded in primary visual cortex.^{76, 77} The strongest oscillatory component of cortex is the well-studied 40Hz gamma band.^{75, 76, 78-80} Other slower components have also been identified including theta (4-8 Hz)^{75, 80, 81}, alpha (8-13 Hz)^{75, 79, 80}, and beta (14-30 Hz).^{75, 79, 80} Although other aspects of cortex have been extensively studied, we know of no studies of the local field potential in postsubiculum. The data presented below suggest that postsubiculum shows local field potential oscillations similar to other aspects of cortex.

As can be seen in Figure 5.3, there were three regions of non-zero correlations: a region showing complex substructure in the low ranges (1-60 Hz), a 130-160 Hz region, and high-frequency components (>200 Hz). The low-frequency region contained a complex substructure including a smaller 5-10 Hz region (theta), and an un-correlated 10 Hz component (non-biological, arising from automated pellet-delivery feeders). In addition, the correlation matrix showed a strong 20-50 Hz (gamma) component. The identification of a 150 Hz fundamental oscillation is novel, but there have been reports of high-frequency oscillations >200 Hz in other aspects of rodent cortex.⁸²⁻⁸⁴ There have been no previous studies of local field potentials in postsubiculum, but the results presented here suggest that postsubiculum shows oscillatory components similar to other aspects of cortex, rather than to hippocampus.

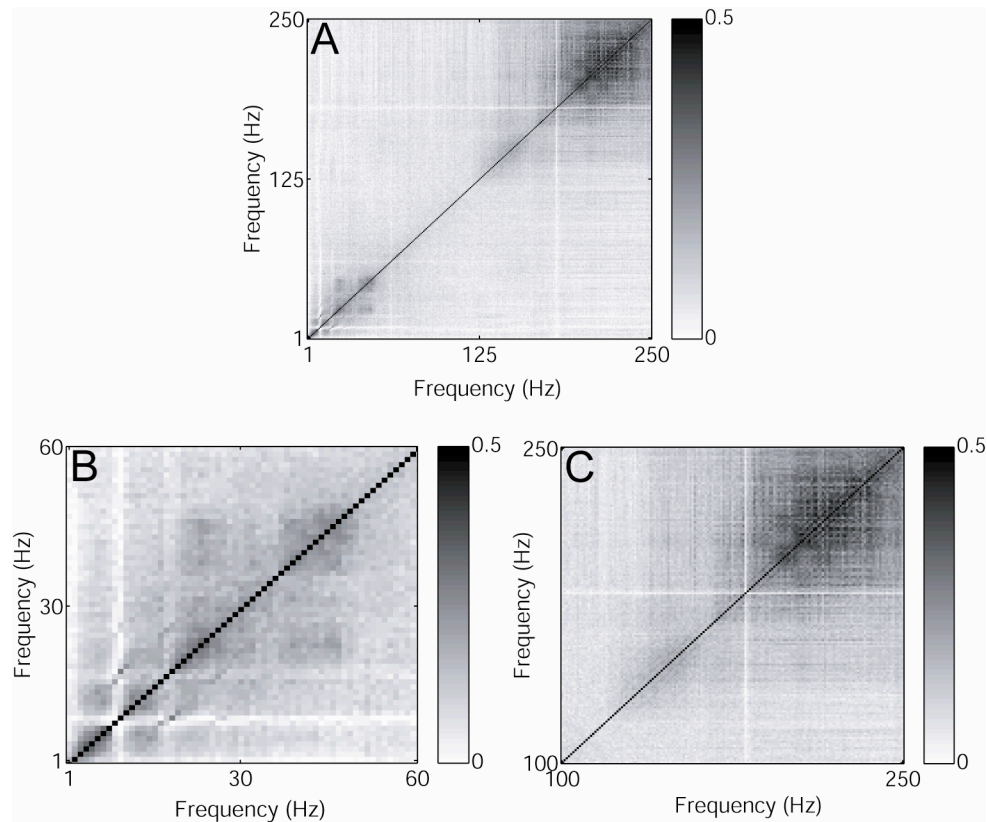


Figure 5.3 Correlation Structure of LFPs Recorded from the Postsubiculum of Two Rats

(A) Correlation matrix of all frequencies ranging from 1 to 250 Hz. Note the regions in the low-frequency range (1–60 Hz) and in the high-frequency range (120–160 Hz), as well as the strong >200 Hz components. (B) Expanded correlation matrix showing the substructure in the low-frequency range. The uncorrelated signal occurring at 10 Hz is non-neural noise generated by the automated pellet-delivery system. (C) Expanded correlation matrix showing the 120–160 Hz component and the >200 Hz component. The uncorrelated signal occurring at 180 Hz is an odd harmonic of the 60 Hz non-neural noise. Figure from Masimore et al, 2004.

5.4.4 Striatum

Fundamental oscillatory frequencies have not been well-studied in the dorsal striatum, however, there have been preliminary reports of striatal rhythms. DeCoteau et al.⁸⁵ found that a theta oscillation (7-10 Hz) can be seen under certain conditions and Berke et al.²⁶ have reported the presence of gamma-band oscillations (35-100 Hz). We

recorded local field potentials from the striatum of five rats running a variety of behavioral tasks.

The correlation matrix (Fig. 5.4) identified two clear regions of important frequencies (1-30 and 50-55 Hz). The lack of off-axis correlations between the two regions indicate that these fluctuators were likely to have been generated by different processes.

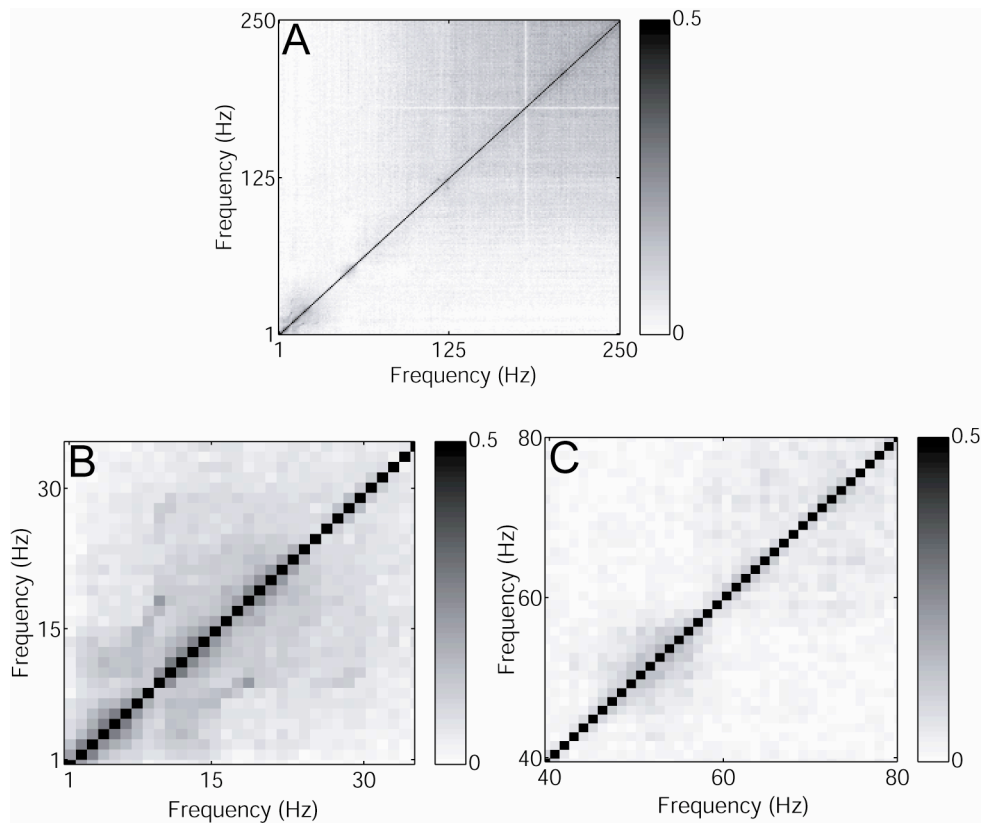


Figure 5.4 Correlation Structure of LFPs Recorded from the Dorsocentral Striatum of Five Rats

(A) Correlation matrix of all frequencies ranging from 1 to 250 Hz. Note the clear blocks in the low-frequency range (1–30 Hz), in the gamma band range (50–55 Hz). (B) Expanded plot showing the substructure in the low-frequency range. (C) Expanded plot showing the tight fluctuator in the mid-frequency range. Figure from Masimore et al, 2004.

Although the correlation matrix does not tell us when the characteristic oscillations appear, nor under what conditions they occur, nor what the behavioral correlates of the frequencies are, it can guide our investigation to look at the fundamental frequencies identified here. The gamma band is traditionally specified as being very broad (30-100 Hz).^{72, 73, 77, 86-88} The data reported here identify the important oscillatory range in striatum as extremely tight (50-55 Hz).

5.5 Discussion

This chapter presents a novel methodology for determining the fundamental frequency of an oscillation within neural time-series, such as the local field potential. By combining two well-understood techniques in common use in neuroscience (Fourier transforms and correlation coefficients), it provides an easily accessible procedure applicable to many aspects of neuroscience. The key advantage over other techniques for determining fundamental underlying frequencies is that it allows the averaging of multiple time windows from long data recordings to filter out noise effects, without making any assumptions about the stationarity of the data. This technique is thus particularly useful for neural data, which tend to be non-stationary and to have a low signal-to-noise ratio.

While the technique of employing correlation coefficients to investigate local field potentials is not new^{75, 89-92}, we make use of a frequently overlooked property of the self-coherence function. Since any peak in the spectral density corresponding to the characteristic frequency of a rhythmic oscillation will have a finite, non-zero width (due to its transient nature), it can be identified by the finite cross-correlations with

neighboring frequencies. The non-stationary, small amplitude aspect of these oscillations would ordinarily be buried in the background noise in a traditional average spectral density. In contrast, correlation coefficients are calculated by summing the correlations over a large number of individual power spectra. This summation leads to a cancellation of uncorrelated positive and negative coefficients, while a true correlated signal is undiluted by the summation process and is thereby readily detected.

5.5.1 Importance for Other Recording Technologies

Neural oscillations appear in many data acquisition paradigms, including EEG, fMRI, MEG, and ensemble neural recordings. The techniques proposed in this chapter are applicable to any time-series and will be of general use for all of these neural data.

5.5.2 Detection of Non-Neural Noise Sources

Any experimental set-up will include spurious non-neural noise arising from external sources. Experimental techniques to control such noise sources (e.g. 60Hz and its harmonics) are a large part of any experimental project. Because these non-neural sources will be uncoupled from real neural fluctuators, they will appear as sharp uncorrelated bands in the correlation plot (e.g see Fig. 5.2). Because non-biological signals tend to be very sharp, the harmonics often also appear in the correlation plots. Off-axis correlations between a signal and its harmonics may suggest that the signal is non-biological. For example, the 100ms pulses used in the automated pellet feeders produced a non-biological 10Hz signal and its corresponding 20Hz harmonic (see Fig. 5.2). Our methodology provides an additional useful tool to distinguish real neural signals

from non-neural noise sources. These signals can be difficult to disambiguate in power spectra.

5.5.3 Relation to Coherence

The expression employed to calculate the correlation coefficient here (Eq. 5.1) is sometimes referred to as coherence in the signal engineering community.⁹⁰ The correlation equation used here is mathematically equivalent to

$$\rho_{xy} = \frac{S_{xy}}{\sqrt{S_{xx}S_{yy}}},$$

used for cross-spectral analysis.^{75, 93, 94} S_{xy} is the cross-spectrum obtained by Fourier transforming the product of a time-dependent quantity $x(t)$ and the complex conjugate of another time-varying quantity $y(t)$, while S_{xx} and S_{yy} are the traditional spectral densities of $x(t)$ and $y(t)$, respectively. Previous use of the coherence function in neuroscience applications has involved cross-correlations between two spatially distinct probes, so that ρ_{xy} provides spatial correlation information.^{72, 75, 77, 89-91, 95} In the present work, we employ the correlation coefficient to analyze the LFP data from a single electrode taking measurements from a single site. In this way the analysis presented here involves the self-coherence of the LFP signal, while previous investigators have studied the mutual-spatial-coherence function.

5.5.4 Relation to Bispectral Analysis

Bispectral analysis is widely used in EEG experiments to obtain information about the relative phases of oscillators.^{75, 96} The methodology proposed here measures correlated changes in the power spectrum obtained by multiplying the Fourier transform

by its complex conjugate. In contrast, in bispectral analysis, the real and imaginary components are considered separately. The bispectrum is a statistical calculation that yields information which is a mixture of amplitude and phase components. The bicoherence measurement provides strictly phase information just as correlation coefficients provide only amplitude information. The two techniques can thus, depending on the physical system, offer complimentary information.

5.5.5 The Choice of Spectral Estimation Techniques

The method presented in this chapter includes two parts: a transformation of a time-series into the frequency domain and a subsequent statistical analysis in the frequency domain. Multi-taper spectral analysis has been proposed as an alternative technique to analyze time-series neurobiological data.^{92,94} The relative merits of various spectral estimation techniques can be compared with respect to their bias and variance properties. The standard power spectrum (also known as the periodogram) is known to have poor bias due to broad power leakage through the spectrum. One way to improve the bias is to multiply the frequency term by a taper chosen to have desirable bias characteristics. While a taper could be almost any well behaved function, the Slepian sequences are often chosen for their independence characteristics.^{92,97,98} A carefully chosen taper function can improve bias, but all tapers cause variance inflation. Multi-taper analysis utilizes the orthogonality of the Slepian sequences to effectively increase the sample set and thus decrease the variance, all while saving the bias improvements of tapering.^{97,98} Although this improves bias, the variance still remains greater than that of the standard transform. In calculating correlation coefficients, the bias term is normalized

out. Thus, improving the bias term does not improve correlations. In contrast, correlations are highly dependent on variance, and thus any inflation of the variance is problematic. For data looking only at first-order measures (such as power spectra) a multi-taper analysis may be a better choice^{78, 92}, but multi-taper analysis does not improve correlation-based measures such as those described here.

5.6 Conclusion

This chapter presented generally-applicable techniques for identifying fundamental fluctuation frequencies in neural time-series data, without any *a priori* filtering assumptions. The proposed technique combines two well-understood neural analysis methods (Fourier transforms and correlation matrices), which will make the technique accessible to many neural data acquisition paradigms and should provide a useful tool for the analysis of neural data.

Chapter 6

50 Hz Oscillations

6.1 Introduction

In many neural structures, transient, synchronous oscillations in the local field potential are correlated with distinct behavioral states. These events are thought to reflect organized neural firing patterns which have implications for information processing.^{13, 15, 99-101} Chapter 5 presented a method for identifying fundamental frequencies within local field potentials.¹⁰² When applied to LFP data in which the key frequencies have been determined from conventional filtering analysis, our method readily identifies those frequencies. When applied to local field potentials recorded from dorsal striatum, it identified 48-58 Hz as an important oscillation frequency.¹⁰² For simplicity, this oscillation will be referred to as γ 50. Using conventional filtering techniques, Berke et al.²⁶ has also reported the presence of LFP power at a similar 50Hz frequency in the striatum of awake rats. While other basal ganglia oscillations have been reported to have behavioral correlates in normal animals^{26, 60, 103}, the behavioral significance of γ 50 is not known. Here it is reported that the γ 50 oscillation occurs in transient \sim 150 ms events that are co-incident with the initiation of movement on spatial tasks.¹⁰⁴

6.2 Cross-Frequency Self-Correlations

The primary data came from rats running two of the behavioral tasks presented in Chapter 4. Seven rats ran the Multiple-T sequential-spatial navigation task and five rats ran the Take-5 sequential non-spatial task. Due to noise present in the early recordings

that overwhelms standard filtering techniques, specific event times could only be identified on 4 of the 7 multiple-T rats. Therefore, data from 7 rats was used for correlation analyses (Figure 6.1) while data from 4 of those 7 was used for speed analyses (Figure 6.4). Details of the tasks, animal care and surgery and general data processing are presented in Chapter 4.

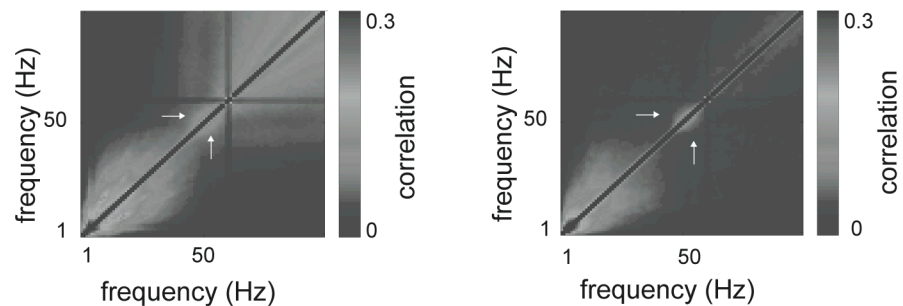


Figure 6.1 Cross-Frequency Self Correlation

Correlations were averaged across tetrodes within each animal, and then across animal.

Important frequencies are indicated by blocks of high correlation surrounding the diagonal. Note the clear signal at 48–58 Hz (white arrows). The zero correlation crossbars at 60 Hz are due to electrical line noise and do not contribute to other correlations. [MT: 7 animals, T5: 5 animals]. Figure from Masimore et al, 2005.

The within-time-series, cross-frequency correlation plot showed a fundamental frequency in the 48-58 Hz range that was clearly distinct from activity at surrounding frequencies (Figure 6.1). While every frequency in a power spectrum is trivially correlated with itself (producing a correlation of 1 on the $x=y$ line), transient coherent oscillations hidden within the spectral density are revealed by their non-zero correlations with frequencies adjacent to the center frequency of the oscillation.^{102, 105} The zero correlation crossbars occurring at 60 Hz in Figure 6.1 were due to electrical line noise and do not contribute to other correlations. As can be see in Figure 6.1, our correlation analysis also indicates oscillatory activity in other ranges, such as theta and beta, which is

consistent with other observations in rodent striatum.^{26, 60} This chapter will concentrate on the γ 50 signal.

To test the hypothesis that this oscillation was associated with a particular behavioral state, we analyzed data from the rats performing the Multiple-T task (7 animals).^{55, 66} In this task, the rat typically runs smoothly through the navigation sequence and stops at the feeders to eat and groom. After remaining at the feeder for a variable length of time, the rat leaves the feeder to self-initiate a new lap. Rats typically remained at the second feeder for a long time (average wait time at the second feeder was 27 sec, 95% CI = [9-45 sec]), but once they left the feeder they ran at a stereotyped speed on a stereotyped path through the navigation sequence (average total lap time from leaving the second feeder to arriving at the first feeder, traveling nearly 4 m was 16 sec, 95% CI = [10 – 22 sec]).^{55, 66}

The task was divided into behaviorally significant regions such as the navigation sequence and the return rails. The 50 Hz correlation block (Figure 6.1) was found to be significantly suppressed during the navigation sequence ($P < .05$, Wilcoxon paired sign-rank, $n_{\text{rat}} = 7$), but not on the return rail portion ($P = .47$, Wilcoxon paired sign-rank, $n_{\text{rat}} = 7$). Rats typically ran smoothly through the navigation sequence while they engaged in a wide range of behaviors on the return rail, including running, grooming, feeding, resting and transitions between these activities.

6.3 Behavioral Correlations of γ 50 Events

Specific events characterized by an increase in the 45-55 Hz band were identified using conventional filtering methods.¹⁰⁶ For a given session, all LFPs were filtered

individually at both 35-45 Hz and 45-55 Hz. Times were identified when the signal power exceeded 7 standard deviations above the mean amplitude for the 45-55 Hz band but not the 35-45 Hz band. As these γ 50 oscillations appear across the striatum, only high power epochs occurring in LFPs from two or more electrodes were included.

Clinical evidence has long suggested that the basal ganglia are involved in volitional movement and, specifically, the initiation of movement.¹⁰⁷⁻¹¹⁰ This led us to focus on motor activity for further analysis. Figures 6.2 and 6.3 show typical examples of a γ 50 oscillation from each task. These events were found primarily (but not exclusively) at the feeders, closely tied to the instant the animal left the feeders. As shown in panel E of Figures 6.2 and 6.3, the animal's speed increased dramatically at the precise moment of the γ 50 oscillation.

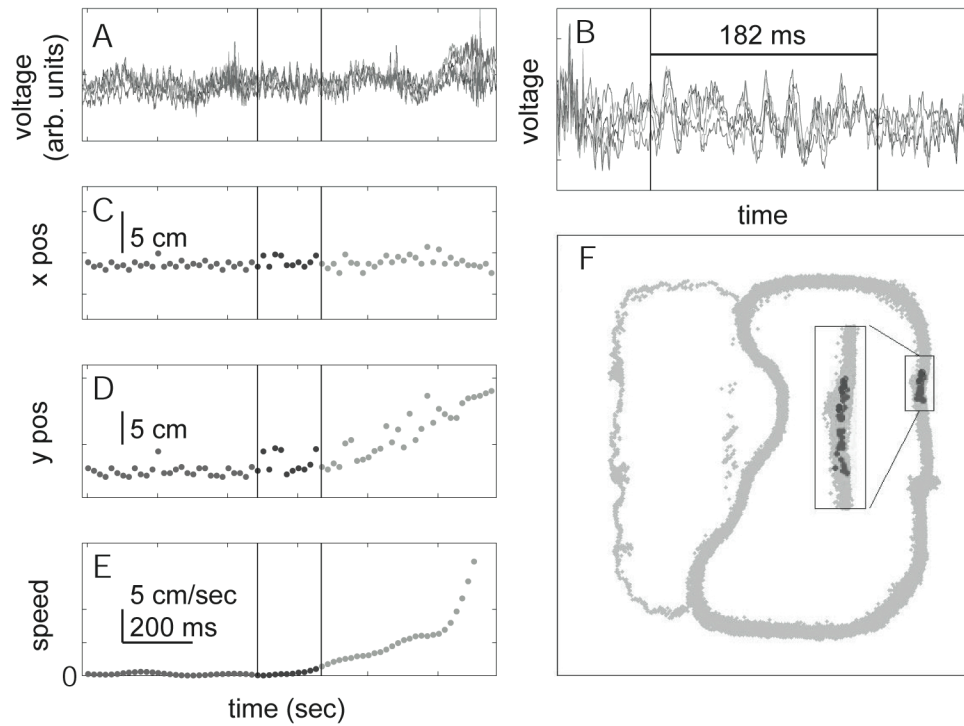


Figure 6.2 Example γ_{50} Event from the Multiple-T Task

The event occurred just as the animal left the first feeder. (A) Raw LFP data. The two vertical lines indicate the identified γ_{50} event. (B) Raw LFP data zoomed in to show the transient synchrony. (C,D) x and y position of the animal. (E) Speed of the animal. (F) The position of the animal just prior to and just after the γ_{50} event. Individual lines in panels A and B are raw LFP signals recorded from different electrodes in a single animal. Panels A and C–E are aligned in time. Figure from Masimore et al, 2005.

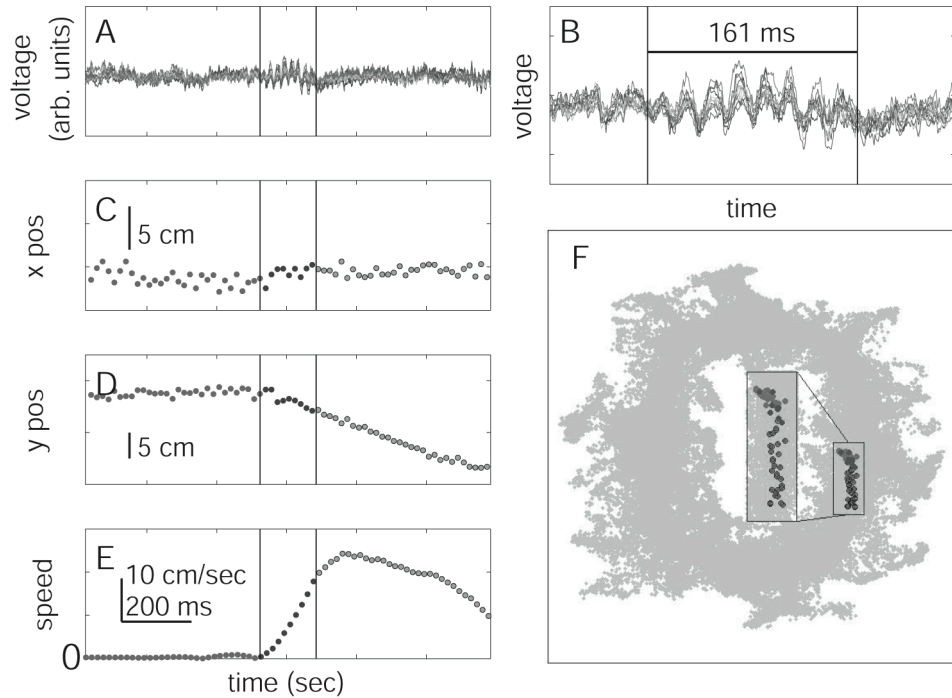


Figure 6.3 Example γ_{50} Event from the Take-5 Task

The event occurred just as the animal left the east feeder. (A) Raw LFP data. The two vertical lines indicate the identified γ_{50} event. (B) Raw LFP data zoomed in to show the transient synchrony. (C,D) x and y position of the animal. (E) Speed of the animal. (F) The position of the animal just prior to and just after the γ_{50} event. Individual lines in panels A and B are raw LFP signals recorded from different electrodes in a single animal. Panels A and C–E are aligned in time. Figure from Masimore et al, 2005.

Once the times of specific events had been identified, traditional behavioral neuroscience methods (such as peri-event time histograms) could be used to analyze behavior based on those times. Given the hypothesized relationship between the basal ganglia and movement initiation, and the observation that many individual events occurred at the time of feeder departure, we hypothesized a relationship between the γ_{50} signal and movement initiation. To test this hypothesis, we constructed a peri-event-time histogram, measuring the speed before and after the signal, aligned with the start-time of

the signal. As shown in Figure 6.4, speed increased dramatically at the time of the γ_{50} event.

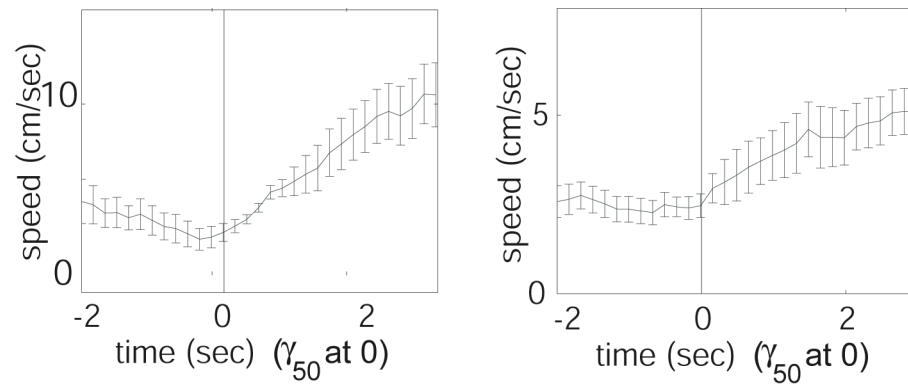


Figure 6.4 Speed Relative to the Time of γ_{50} Events

Specific γ_{50} events were identified as described in the Chapter 5. Speed measurements were aligned to the time of the γ_{50} event and averaged first within session (MT: 88 ± 43 events per session; T5: 94 ± 117 events per session.), then within animal (MT: 8.7 ± 6.9 sessions per animal; T5: 6.4 ± 1.8 sessions per animal) and finally across animals (MT: 4 animals; T5: 5 animals), producing a peri-event histogram. Error bars indicate SE measurements across animals. Figure from Masimore et al, 2005.

Short duration, frequency-focused LFP events, characterized by synchrony across large spatial areas, have been associated with periods of motor activity and visual perception.^{60, 77, 99, 101} The γ_{50} event described here is phenomenologically similar in that it is characterized by transient oscillatory activity at 48 – 58 Hz, with a duration of 100-150 ms and showing synchrony across a relatively large spatial scale (> 1 mm). It is possible that the γ_{50} event may arise from striatal neural activity involved in the self-initiation of movement, particularly a well-trained ballistic movement. This transiently synchronous signal may provide a key to understanding striatal function. As diseases of the basal ganglia involve aberrant oscillatory states^{103, 111, 112}, striatal oscillations in

normal animals may shed light on changes in information processing that accompany changes in oscillatory activity in basal ganglia diseases.

6.4 Conclusions

An oscillatory local field potential event (γ 50) has been identified in striatum. It is characterized by transient oscillatory activity at 48-58 Hz, with a duration of 100-150 ms and showing synchrony across a large spatial scale (> 1 mm). A strong increase in speed was found to occur at the moment of these events on rats running multiple tasks.

Chapter 7

Future Directions and Open Questions

7.1 Introduction

The work discussed in the previous chapters leads to a number of future research directions and also leaves several open questions. Several of the future directions were discussed elsewhere, and are gathered here to highlight the variety of research directions that have grown out of what was initially an exploratory project. The open questions remain after a number of preliminary experiments that provide some insight into the origin and functional significance of the 50 Hz oscillations discussed in chapter 6.

7.2 Fluctuator Simulation

The first model discussed in chapter 3, a distribution of Poisson fluctuators, has found success in a wide variety of systems⁶⁹ and is a logical starting point for examining $1/f$ noise in a novel system, such as LFPs. Local field potentials do not directly map onto this model, but given that the model's resulting power spectrum is fairly insensitive to underlying parameters, as show in Fig 3.4, it is reasonable to try to simulate LFPs with biologically relevant modifications. A first attempt may be that discussed in section 3.2. Synaptic fluctuations are well described by alpha functions (eq. 3.6) and τ has been measured in a variety of systems.³⁴ It would be interesting to determine the slope of the power spectrum resulting from a signal generated by placing alpha functions at random times. There may be a way to model the temporal aspects of alpha functions in a more physiologically relevant way than as a random distribution. As the theoretical basis of

local field potentials is explored further, additional types of fluctuation phenomena could be incorporated into this simulation.

7.3 Dielectric Properties of Brain Tissue

The dielectric properties of brain tissue could contribute to the observed power spectra of local field potentials.¹¹³ The frequency dependence of the conductance and permittivity of tissue in different brain structures would need to be measured, using a system very similar to that used in traditional recording experiments. Ideal experiments will use deeply-anesthetized, intact animals and the same probes used for recording experiments. Should it prove experimentally difficult to directly measure the conductance and permittivity, it may be useful to inject white noise at one location and measure the transmitted signal at various distances away from the noise source. If the transmitted signal shows a power spectrum similar to those observed for LFPs, it could suggest that the dielectric properties of the local tissue play a significant role in the structure of recorded signals.

The experimental set-up used to measure the dielectric properties of brain tissue could also be used to test a specific hypothesis related to the 50 Hz oscillations discussed in chapter 6. Berke suggested that striatal 50 Hz oscillations are generated in the piriform cortex,²⁸ a laminar structure associated with olfactory information processing. This hypothesis could be tested by inserting an electrode into piriform cortex, stimulating at 50 Hz, and recording the transmitted electrical activity at locations across striatum. We observe that 50 Hz oscillations are strongest in the ventral medial portion of striatum and diminish in power when moving towards the dorsal lateral striatum. If striatal 50 Hz

oscillations are generated in piriform cortex and volume conducted to striatum, a stimulation experiment should produce the same power distribution across striatum.

7.4 Self-Organized Criticality

Section 3.4 discussed self-organized criticality (SOC) and its potential applicability to local field potentials, which can be explored theoretically and experimentally. To develop an SOC-based model for local field potentials, researchers will need to carefully examine ideas such as critical states and avalanches in the context of LFPs. There is no immediately obvious physical substrate for these ideas, but perhaps further theoretical explorations of LFPs could highlight candidate mechanisms. *Self-Organized Criticality: Emergent Complex Behavior in Physical and Biological Systems* by Henrik Jensen⁴⁹ provides a discussion of numerous self-organized criticality based models and will provide a solid foundation for researchers attempting to pursue self-organized criticality as an explanation for the observed power law spectral behavior of LFPs.

The relevant experiments are conceptually simple but may prove challenging to perform in a system similar to those used for traditional LFP recording experiments. It will first be necessary to obtain an LFP time series that is free of all known external noise sources as the data analysis that follows is extremely sensitive to spurious fluctuations. O'Brien and Weissman outline an analytical technique to identify self-organized criticality⁵⁰ and then applied the technique to experimental data⁵¹, warning of several potential pitfalls. In brief, as fluctuations in a SOC system are triggered by an external, adjustable parameter (for example, a sandpile at the angle of maximum stability will not

avalanche until an additional grain of sand is added), O'Brien and Weissman argue that a signature of SOC is a non-zero imaginary component of the noise second spectrum. That is, there should be a "phase-lag" in the fluctuation spectrum (first spectrum) that will be revealed by examination of higher order moments of the spectral density.

7.5 Relation to Other Dynamic Neural Signals

Section 1.2 discussed the relationship between LFPs and other electrodynamic neural signals, spikes and EEG. All three of these signals reflect underlying voltage fluctuations, but at different spatial and temporal scales. Another recording technology, functional magnetic resonance imaging (fMRI) records a signal related to cerebral blood flow. When neurons fire action potentials, they consume oxygen carried by hemoglobin in red blood cells, which results in an increase in blood flow to the locally active region.¹¹⁴ This change in blood-flow and oxygenation is reflected in the blood oxygen level-dependent signal (BOLD) that is recorded in fMRI. Functional magnetic resonance imaging is a useful tool for non-invasive imaging of the human brain and an understanding of how the BOLD signal relates to electrodynamic neural signals such as LFPs, spikes, and EEG would allow for greater integration of research results obtained through different techniques. Recent studies show that the fMRI BOLD signal is more closely related to LFPs than spiking,¹¹⁴ and thus an increased understanding of local field potentials could improve the interpretation of data obtained by fMRI.

7.6 γ 50 Oscillations

7.6.1 Origin of Oscillations

Upon recording a novel local field oscillation, it is desirable to verify that the oscillation was generated in the brain structure where the electrodes were placed, rather than the result of the passive spread of currents generated in other brain structures. This has proven to be challenging in the case of the 50 Hz striatal oscillations described in Chapters 5 and 6.

Traditional methods used to prove the local origin of an LFP oscillation are based on the interpretation of oscillations arising in structures with a laminar cellular arrangement. Current source density experiments²³⁻²⁵, discussed in section 2.4.1, can identify sources and sinks of extracellular currents, which can then be associated with the underlying cellular anatomy. The high spatial precision necessary to perform this analysis makes it impractical to perform these experiments in awake, behaving animals. Another approach that can be applied to data recorded from awake, behaving animals is to search for phase shifts among oscillations recorded from spatially separated electrodes within the same structure. These phase shifts would not be expected from volume conducted oscillations and indicate that a current sink or source is located between the relevant electrodes. Such a method has been used to verify the local origin of oscillations recorded in the subthalamic nucleus and pallidum, two non-laminar brain structures that are part of the basal ganglia.¹¹⁵ Such phase shifts have not been observed in 50 Hz striatal oscillations, which appear coherent across the entire recorded region.

A second approach to verify the local origin of an LFP oscillation is based on the assumption that local field potentials reflect synaptic activity and that this synaptic activity that is correlated with extracellular spikes. Most experiments, including all of the ones discussed in chapters 4-6, record both the local field potentials and spikes, thus enabling the researcher to search for correlations between the two signals. There are numerous ways in which the two signals could be correlated. For example, high-voltage spindles are a type of LFP oscillation that occur in awake, immobile animals.²⁶ There are different types of cells within striatum and it has been shown that one cell type tends to spike just before the peak of high voltage spindles, while another cell type tends to spike approximately 45° after the high voltage spindle peak. One can easily imagine other possible correlations, such as cells that fire at the beginning of an oscillatory burst or at some multiple of the local field oscillatory frequency. The wide range of correlation possibilities can result in a nearly endless search for a correlation as one cannot prove that the two signals are not correlated, merely that they are not correlated in any of the ways that have been examined. Another possibility is that the local field potentials reflect local synaptic activity, but that correlated cellular spiking is from cells in a distant structure that project to the recording location.

We recorded from a number of candidate brain structures, searching for both 50 Hz oscillations and cells that show correlated firing with 50 Hz oscillations. Figure 7.1 shows the regions where 50 Hz oscillations were not observed, as well as the observed gradient of 50 Hz oscillation strength within striatum. Lateral septum, a medial brain structure associated with movement initiation, showed no 50 Hz oscillations throughout

the entire depth of the brain (1 rat). This suggests that the oscillations are not volume conducted from piriform cortex, as this would not result in an abrupt drop off in 50 Hz oscillations between medial striatum and lateral septum. We also recorded both local field potentials and spikes from motor cortex (1 rat). This structure is both associated with, and projects to, the regions of striatum that show high power 50 Hz oscillations. We found neither 50 Hz oscillations or spike activity that correlates with 50 Hz oscillations.

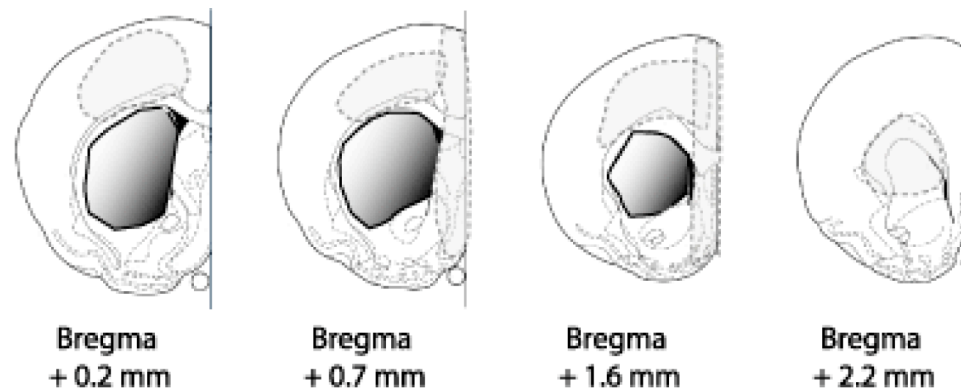


Figure 7.1 Recording Locations.

We recorded from a number of brain structures in an attempt to locate the origin of the γ 50 events that were described in Chapter 6. Shaded areas indicate locations from which we have observed 50 Hz; areas outlined with a dashed line indicate locations from which we have recorded and do not observe 50 Hz. Recorded areas include dorsal and medial striatum, motor cortex, lateral septum, and pallidum. Within striatum, oscillations are strongest in the ventral-medial area, as indicated by the shaded gradient.

Despite these negative results, there is considerable evidence that suggest that LFP oscillations can be locally generated in non-laminar structures such as striatum. Striatal high voltage spindles were mentioned above and DeCoteau et al. have identified locally generated theta oscillations in rodent striatum.²⁷ Other non-laminar basal ganglia structures also show locally generated oscillations.^{26, 60, 116-118} A robust theory of local field potentials that includes parameters related to cellular architecture and to the

underlying fluctuation phenomena beyond synaptic fluctuations would help guide experiments that could conclusively demonstrate that 50 Hz oscillations are generated in striatum.

7.6.2 Dopamine

The experiments discussed thus far all entail recording from healthy animals and correlating neural activity with various behavioral parameters. Neuropharmacology is an experimental approach that involves studying drug-induced changes in the functioning of neurons. Dopamine is a major neurotransmitter in the striatum (and elsewhere) and cells that use dopamine as a transmitter are involved in motor control circuits. As discussed in chapter 6, we observed a correlation of 50 Hz events with a motor control event (initiation) and thus we hypothesized that interfering with the striatal dopamine system would alter 50Hz events.

There are several indications that the dopamine system could be involved in striatal 50 Hz oscillations. The striatum is one portion of the basal ganglia, a brain structure involved in disease processes such as Parkinson's disease. Oscillatory activity in the human basal ganglia has also been studied through LFPs recorded after microelectrode implantation for the treatment of Parkinson's disease and dystonia. When withdrawn from dopaminergic therapy, oscillatory activity is synchronized into three major frequency bands. The lowest band (3 – 12 Hz) is in the frequency range of parkinsonian rest and action tremor.^{119, 120} Beta-band oscillations (~13 – 32 Hz) are a prominent feature of LFPs recorded in both subthalamic nucleus (STN) and globus pallidus (GPi) of parkinsonian patients.^{115, 121-124} These oscillations are coherent between

the two structures and are viewed as a characteristic of basal ganglia circuitry in Parkinson's disease.^{111, 115, 125, 126} Gamma band activities (here, 65-85 Hz) have also been reported in both STN and GPi^{115, 125} along with very high frequency activity (200-300 Hz) in STN.¹²⁷ Some of the oscillations recorded in the diseased human basal ganglia show distinct changes between when patients are on dopaminergic therapy and when drug therapy is withdrawn. There are multiple reports that beta band activity is suppressed as motor symptoms improve after the administration of drug therapy.^{115, 124, 125, 128} The suppression of the beta activity occurs prior to and during voluntary movements and following environmental cues related to future movement demands. Thus, in the treated human basal ganglia, modulation of oscillatory activity is well correlated with motor-related activity while the diseased human basal ganglia shows persistent, non-modulated beta band activity. The modulation of beta activity in drug treated humans shows striking resemblance to the beta activity observed in healthy monkeys.⁶⁰

There is an extensive history of behavioral experiments with both reversible systemic dopamine manipulations and permanently damaged dopamine systems.¹²⁹ There are relatively few electrophysiology studies under these paradigms. In 1-methyl 4-phenyl 1,2,3,6-tetrahydropyridine (MPTP) treated monkeys (in which the dopaminergic system is damaged and animals present many common symptoms of Parkinson's disease¹³⁰), basal ganglia cells (STN and GPi) tend to fire in synchrony as opposed to the independent firing observed in normal animals.^{118, 126, 131, 132} The beta oscillations present in healthy monkey striatum have not been studied in a dopamine manipulated system. Rat

STN has been studied in anaesthetized 6-Hydroxydopamine (6-OHDA) lesioned rats, in which the dopaminergic system is damaged.^{133, 134} In lesioned rats, spikes were found to cluster into bursts more than in normal animals and showed more synchrony and a consistent phase relationship with the LFP. Work has also been done with dopamine transporter knock-out mice (a model system that allows for inducible and reversible manipulations to the dopamine system) where it is found that LFP power in the theta (4.5 – 9 Hz) and gamma (30 – 55 Hz) bands increases relative to that in the delta (1.5 – 4 Hz) and beta (11 – 30 Hz) bands during periods of excessive movement and dopamine depletion.^{135, 136} Local field potentials have also been studied in the STN of alert, healthy rats.¹⁰³ Following application of the D2 agonist quinpirole, the power in the 40-80 Hz band was found to increase significantly. In this study, the increased power in the gamma band was verified to be of local origin as it was not observed on electrodes found to be outside, but near to, the subthalamic nucleus.

We conducted preliminary experiments to examine striatal 50 Hz oscillations under the effects of dopamine receptor agonists and antagonists (1 rat). There are two different types of dopamine responsive cells - those that have D1 receptors and those that have D2 receptors. Agonists activate the receptors while antagonists block the receptors. We applied drugs systemically, using saline injections on alternate days as an experimental control. The drugs were SKF38393 (D1 agonist), SCH23390 (D1 antagonist), quinpirole (D2 agonist), and sulperide (D2 antagonist). Results of these experiments are shown in Fig 7.2.

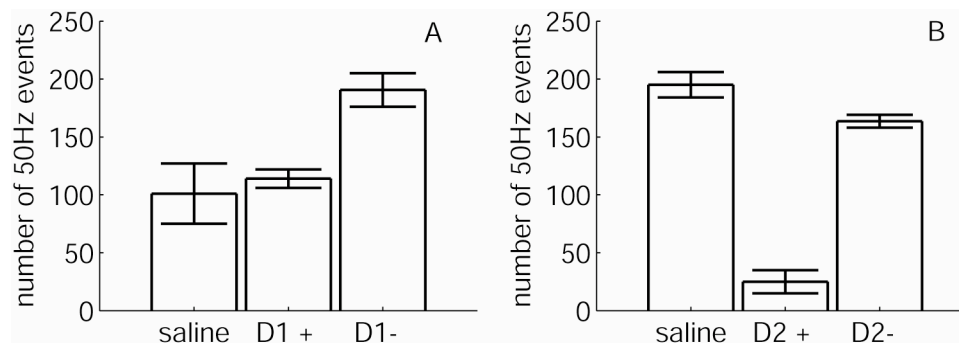


Figure 7.2 Preliminary Data of Dopamine Manipulations

We conducted preliminary experiments to examine striatal 50 Hz oscillations under the effects of dopamine receptor agonists (+) and antagonists (-). The error bars are standard error over two trials. (A) D1 antagonists significantly increase the number of 50 Hz events recorded during each 40 min. session. (B) D2 agonists significantly decrease the number of 50 Hz events recorded during each session.

The systemically applied dopaminergic drugs had a significant effect on the number of 50 Hz events recorded during behavioral tasks. It is difficult to interpret the results, as systemic drugs affect dopamine receptors throughout the body, not just in the structure under study. Animals showed significant behavioral changes, including running no laps under the application of the D1 antagonist. A properly designed experiment would start with a series of dose-response experiments with the behavioral tasks to be used in the subsequent recording experiments. Completing all of the necessary controls for the behavior, pharmacology, and electrophysiology portions of this experiment is conceptually simple but extremely labor intensive and will require a large number of animals. Other experimental approaches, such as dopamine transporter knock-out mice

may be a better way to approach the open question of how dopamine is involved in striatal 50 Hz oscillations.

Brown et al have recorded from the subthalamic nucleus of healthy rats and observed power in the gamma frequency band that increases under the application of quinpirole. It would be interesting to compare the oscillations in striatum and STN. We attempted to record from STN (2 animals) but were unable to place electrodes into the structure using the standard recording device and techniques used for other experiments. Recording from both structures under the same conditions is necessary for direct comparison. Alternative recording technologies, including ones currently in the early stages of development, may provide more successful ways to target small structures such as STN.

Chapter 8

Summary

Neurological local field potentials are characterized by apparently random fluctuations that are interspersed with periods of clear oscillatory activity. It is commonly thought that LFPs reflect the electrical fluctuations occurring at synapses between neurons. This theory stems from experiments performed in structures where the cellular arrangement is laminar and fails to account for the occurrence of LFP oscillations in structures that do not possess regular cellular arrangements. The power spectrum of a typical local field potential recording shows a power-law frequency dependence. Numerous mathematical theories have been developed that describe the power spectrum that results from different fluctuation phenomena, but they have not previously been applied to local field potentials.

One of the more versatile frameworks for obtaining $1/f$ power spectra is based on systems being comprised of numerous two state Poisson fluctuators that show a distribution of relaxation times. This model does not neatly map onto local field potentials, but modifications that account for physiologically relevant fluctuations could be explored through simulations. The extracellular medium is extremely heterogeneous and could act as a frequency dependent filter of electrical fluctuations. Experimental measurements of the conductivity and permittivity of the extracellular medium could help to determine the impact of the extracellular dielectric properties on the observed LFP power spectrum. Further examination of the applicability of these theories to local field

potentials could help to develop a robust theory of LFP fluctuations that could account for phenomena observed in both laminar and non-laminar structures.

Typical LFP experiments entail examining long time series of voltage fluctuations. A simple technique, combining Fourier transforms and correlation coefficients has been shown to yield unambiguous determinations of the frequencies without *a priori* filtering. This procedure also provides quantitative information concerning interactions between activity at different frequencies. This technique identified the characteristic frequencies of known oscillations in hippocampus and cortex. Application to dorsal striatal LFPs identified a low-frequency theta component as well as a narrow gamma band oscillation at 50-55 Hz. These coherent oscillations, which we term γ_{50} , occurred in brief (150 ms) events co-incident with the initiation of movement. On navigation tasks, the animal's speed increased dramatically at the precise moment of the γ_{50} event.

This work leads to a number of future directions and open questions. Future directions include developing a theoretical framework for local field potential fluctuations that integrates with the theoretical basis of other neurodynamic signals. Preliminary experiments suggest that γ_{50} events are generated in the striatum, but this has not been verified. We hypothesized that interfering with the striatal dopamine system would alter γ_{50} events and preliminary data suggests that this is true. Improved recording technologies and alternative experimental paradigms could be used to further explore this hypothesis.

References

- 1 P. L. Nunez and R. Srinivasan, *Electric fields of the brain : the neurophysics of EEG* (Oxford University Press, Oxford ; New York, 2006).
- 2 J. I. Hubbard, R. Llinás, and D. M. J. Quastel, *Electrophysiological analysis of synaptic transmission* (Williams & Wilkins Co., Baltimore,, 1969).
- 3 C. Bedard, H. Kroger, and A. Destexhe, *Physical Review Letters* **97** (2006).
- 4 G. Buzsaki, *Neuron* **33**, 325 (2002).
- 5 A. Kamondi, L. Acsady, X. J. Wang, and G. Buzsaki, *Hippocampus* **8**, 244 (1998).
- 6 P. Dutta and P. M. Horn, *Reviews of Modern Physics* **53**, 497 (1981).
- 7 M. B. Weissman, *Reviews of Modern Physics* **60**, 537 (1988).
- 8 B. Neumcke, *Biophys Struct Mech* **4**, 179 (1978).
- 9 B. Pilgram and D. T. Kaplan, *Am J Physiol* **276**, R1 (1999).
- 10 W. S. Pritchard, *Int J Neurosci* **66**, 119 (1992).
- 11 M. Nakata and K. Mukawa, *Pavlov J Biol Sci* **24**, 90 (1989).
- 12 J. O'Keefe and L. Nadel, *The hippocampus as a cognitive map* (Oxford University Press, Oxford, 1978).
- 13 C. H. Vanderwolf, *Psychol Rev* **78**, 83 (1971).
- 14 A. Ylinen, A. Bragin, Z. Nadasdy, G. Jando, I. Szabo, A. Sik, and G. Buzsaki, *J Neurosci* **15**, 30 (1995).
- 15 G. Buzsaki and A. Draguhn, *Science* **304**, 1926 (2004).
- 16 J. B. Johnson, *Physical Review* **32**, 97 (1928).
- 17 H. Nyquist, *Physical Review* **32**, 110 (1928).
- 18 C. Parman and J. Kakalios, *Physical Review Letters* **67**, 2529 (1991).
- 19 D. M. Liou, J. Gong, and C. C. Chen, *Japanese Journal of Applied Physics Part 1- Regular Papers Short Notes & Review Papers* **29**, 1283 (1990).
- 20 J. S. Buchwald, E. S. Halas, and S. Schramm, *Electroencephalography and clinical neurophysiology* **21**, 227 (1966).

- 21 G. H. Fromm and H. W. Bond, *Electroencephalography and clinical*
neurophysiology **17**, 520 (1964).
- 22 G. H. Fromm and H. W. Bond, *Electroencephalography and clinical*
neurophysiology **22**, 159 (1967).
- 23 J. A. Freeman and C. Nicholson, *Journal of neurophysiology* **38**, 369 (1975).
- 24 U. Mitzdorf, *Physiol Rev* **65**, 37 (1985).
- 25 C. Nicholson and J. A. Freeman, *Journal of neurophysiology* **38**, 356 (1975).
- 26 J. D. Berke, M. Okatan, J. Skurski, and H. B. Eichenbaum, *Neuron* **43**, 883
(2004).
- 27 W. E. DeCoteau, C. Thorn, D. J. Gibson, R. Courtemanche, P. Mitra, Y. Kubota,
and A. M. Graybiel, *Journal of neurophysiology* **97**, 3800 (2007).
- 28 J. D. Berke, in *The Basal Ganglia VIII*, edited by J. P. Bolam, C. A. Ingham and
P. J. Magill (Springer Science and Business Media, New York, 2005).
- 29 G. Buzsaki, R. G. Bickford, G. Ponomareff, L. J. Thal, R. Mandel, and F. H.
Gage, 1988), Vol. 8, p. 4007.
- 30 K. Nagata, E. Sasaki, K. Goda, N. Yamamoto, M. Sugino, K. Yamamoto, I.
Narabayashi, and T. Hanafusa, *Clinical physiology and functional imaging* **26**, 92
(2006).
- 31 J. S. Jeong, *Clinical Neurophysiology* **115**, 1490 (2004).
- 32 A. P. Georgopoulos, et al., *Journal of neural engineering* **4**, 349 (2007).
- 33 F. J. Langheim, A. C. Leuthold, and A. P. Georgopoulos, *Proceedings of the*
National Academy of Sciences of the United States of America **103**, 455 (2006).
- 34 B. Hille, *Ion channels of excitable membranes* (Sinauer, Sunderland, Mass.,
2001).
- 35 C. R. Anderson and C. F. Stevens, *The Journal of physiology* **235**, 655 (1973).
- 36 C. F. Stevens, *Biophysical journal* **12**, 1028 (1972).
- 37 A. K. Jonscher, *Nature* **267**, 673 (1977).
- 38 C. Gabriel, S. Gabriel, and E. Corthout, *Physics in Medicine and Biology* **41**,
2231 (1996).

- 39 S. Gabriel, R. W. Lau, and C. Gabriel, *Physics in Medicine and Biology* **41**, 2251
(1996).
- 40 S. Gabriel, R. W. Lau, and C. Gabriel, *Physics in Medicine and Biology* **41**, 2271
(1996).
- 41 A. van Harreveld and S. Ochs, 1956), Vol. 187, p. 180.
- 42 E. Sykova, *Neuroscience* **129**, 861 (2004).
- 43 E. Sykova, *Neurochem Int* **45**, 453 (2004).
- 44 E. Sykova and L. Vargova, *Neurochemistry International* **52**, 5 (2008).
- 45 W. Kilb, P. W. Dierkes, E. Sykova, L. Vargova, and H. J. Luhmann, *Journal of
neuroscience research* **84**, 119 (2006).
- 46 E. Sykova, T. Roitbak, T. Mazel, Z. Simonova, and A. R. Harvey, *Neuroscience*
91, 783 (1999).
- 47 E. Sykova, I. Vorisek, T. Antonova, T. Mazel, M. Meyer-Luehmann, M. Jucker,
M. Hajek, M. Ort, and J. Bures, *Proceedings of the National Academy of Sciences
of the United States of America* **102**, 479 (2005).
- 48 P. Bak, C. Tang, and K. Wiesenfeld, *Physical Review Letters* **59**, 381 (1987).
- 49 H. J. Jensen, *Self-organized criticality : emergent complex behavior in physical
and biological systems* (Cambridge University Press, New York, 1998).
- 50 K. P. O'Brien and M. B. Weissman, *Physical Review A* **46**, R4475 (1992).
- 51 K. P. O'Brien and M. B. Weissman, *Physical Review E* **50**, 3446 (1994).
- 52 J. Jackson and A. D. Redish, *Hippocampus* **17**, 1209 (2007).
- 53 J. C. Jackson, A. Johnson, and A. D. Redish, *J Neurosci* **26**, 12415 (2006).
- 54 N. Schmitzer-Torbert and A. D. Redish, *Archives italiennes de biologie* **140**, 295
(2002).
- 55 N. Schmitzer-Torbert and A. D. Redish, *Journal of neurophysiology* **91**, 2259
(2004).
- 56 A. Johnson, K. Seeland, and A. D. Redish, *Hippocampus* **15**, 86 (2005).
- 57 A. D. Redish, *Beyond the cognitive map : from place cells to episodic memory*
(MIT Press, Cambridge, Mass., 1999).
- 58 J. S. Taube, R. U. Muller, and J. B. Ranck, Jr., *J Neurosci* **10**, 436 (1990).

- 59 R. U. Muller, J. B. Ranck, Jr., and J. S. Taube, *Current opinion in neurobiology* **6**,
196 (1996).
- 60 R. Courtemanche, N. Fujii, and A. M. Graybiel, *J Neurosci* **23**, 11741 (2003).
- 61 N. Schmitzer-Torbert, Univeristy of Minnesota, 2004.
- 62 J. O'Keefe and M. L. Recce, *Hippocampus* **3**, 317 (1993).
- 63 A. V. Olypher, P. Lansky, and A. A. Fenton, *Neuroscience* **111**, 553 (2002).
- 64 R. U. Muller, J. L. Kubie, and J. B. Ranck, Jr., *J Neurosci* **7**, 1935 (1987).
- 65 J. S. Taube, R. U. Muller, and J. B. Ranck, Jr., *J Neurosci* **10**, 420 (1990).
- 66 N. Schmitzer-Torbert and A. D. Redish, *Archives italiennes de biologie* **140**, 295
(2002).
- 67 J. Jackson, N. C. Schmitzer-Torbert, and A. D. Redish, in *Society for
Neurosciences*, 2002).
- 68 F. Janabi-Sharifi, V. Hayward, and C. S. J. Chen, *Ieee Transactions on Control
Systems Technology* **8**, 1003 (2000).
- 69 S. Kogan, *Electronic noise and fluctuations in solids* (Cambridge University
Press, Cambridge [England] ; New York, NY, USA, 1996).
- 70 G. M. Khera and J. Kakalios, *Physical Review B* **56**, 1918 (1997).
- 71 G. Buzsaki, L. W. S. Leung, and C. H. Vanderwolf, *Brain Research Reviews* **6**,
139 (1983).
- 72 A. Bragin, G. Jando, Z. Nadasdy, J. Hetke, K. Wise, and G. Buzsaki, *Journal of
Neuroscience* **15**, 47 (1995).
- 73 J. Csicsvari, B. Jamieson, K. D. Wise, and G. Buzsaki, *Neuron* **37**, 311 (2003).
- 74 J. J. Chrobak, A. Lorincz, and G. Buzsaki, *Hippocampus* **10**, 457 (2000).
- 75 E. Niedermeyer and F. H. Lopes da Silva, *Electroencephalography : basic
principles, clinical applications, and related fields* (Williams & Wilkins,
Baltimore, Md., 1998).
- 76 C. M. Gray and W. Singer, *Proceedings of the National Academy of Sciences of
the United States of America* **86**, 1698 (1989).
- 77 W. Singer and C. M. Gray, *Annual Review of Neuroscience* **18**, 555 (1995).

- 78 B. Pesaran, J. S. Pezaris, M. Sahani, P. P. Mitra, and R. A. Andersen, *Nature Neuroscience* **5**, 805 (2002).
- 79 T. Schanze and R. Eckhorn, *International Journal of Psychophysiology* **26**, 171 (1997).
- 80 T. V. Sowards and M. A. Sowards, *International Journal of Psychophysiology* **32**, 35 (1999).
- 81 M. J. Kahana, D. Seelig, and J. R. Madsen, *Current opinion in neurobiology* **11**, 739 (2001).
- 82 D. S. Barth, *Journal of Neuroscience* **23**, 2502 (2003).
- 83 F. O. Grenier, I. Timofeev, and M. Steriade, *Journal of neurophysiology* **86**, 1884 (2001).
- 84 M. S. Jones and D. S. Barth, *Journal of neurophysiology* **82**, 1599 (1999).
- 85 W. DeCoteau, R. Courtemanche, Y. Kubota, and A. M. Graybiel, in *Society for Neurosciences*, 2002).
- 86 S. Friedman-Hill, P. E. Maldonado, and C. M. Gray, *Cerebral Cortex* **10**, 1105 (2000).
- 87 K. M. Gothard, K. L. Hoffman, F. P. Battaglia, and B. L. McNaughton, *Journal of Neuroscience* **21**, 7284 (2001).
- 88 E. Rodriguez, N. George, J. P. Lachaux, J. Martinerie, B. Renault, and F. J. Varela, *Nature* **397**, 430 (1999).
- 89 L. A. Baccala and K. Sameshima, *Biological Cybernetics* **84**, 463 (2001).
- 90 W. A. Gardner, *Signal Processing* **29**, 113 (1992).
- 91 B. Kocsis, A. Bragin, and G. Buzsaki, *Journal of Neuroscience* **19**, 6200 (1999).
- 92 P. P. Mitra and B. Pesaran, *Biophysical journal* **76**, 691 (1999).
- 93 D. A. Leopold, Y. Murayama, and N. K. Logothetis, *Cerebral Cortex* **13**, 422 (2003).
- 94 R. R. Llinas, U. Ribary, D. Jeanmonod, E. Kronberg, and P. P. Mitra, *Proceedings of the National Academy of Sciences of the United States of America* **96**, 15222 (1999).

- 95 W. H. R. Miltner, C. Braun, M. Arnold, H. Witte, and E. Taub, *Nature* **397**, 434
(1999).
- 96 J. C. Sigl and N. G. Chamoun, *Journal of Clinical Monitoring* **10**, 392 (1994).
- 97 D. B. Percival and A. T. Walden, *Spectral analysis for physical applications :
multitaper and conventional univariate techniques* (Cambridge University Press,
Cambridge ; New York, NY, 1993).
- 98 D. J. Thomson, *Proceedings of the IEEE* **70**, 1055 (1982).
- 99 A. K. Engel, P. Fries, and W. Singer, *Nat Rev Neurosci* **2**, 704 (2001).
- 100 A. A. Kuhn, D. Williams, A. Kupsch, P. Limousin, M. Hariz, G. H. Schneider, K.
Yarrow, and P. Brown, *Brain* **127**, 735 (2004).
- 101 W. Singer, *Nature* **397**, 391 (1999).
- 102 B. Masimore, J. Kakalios, and A. D. Redish, *J Neurosci Methods* **138**, 97 (2004).
- 103 P. Brown, A. Kupsch, P. J. Magill, A. Sharott, D. Harnack, and W. Meissner, *Exp
Neurol* **177**, 581 (2002).
- 104 B. Masimore, N. C. Schmitzer-Torbert, J. Kakalios, and A. D. Redish,
Neuroreport **16**, 2021 (2005).
- 105 B. Masimore, J. Kakalios, and A. D. Redish, in *Fluctuations and Noise in
Biological, Biophysical and Biomedical systems*, edited by S. M. Bezrukov, H.
Frauenfelder and F. Moss (Proceedings of SPIE, Bellingham WA, 2003), p. 224.
- 106 J. Csicsvari, H. Hirase, A. Czurko, A. Mamiya, and G. Buzsaki, *J Neurosci* **19**,
RC20 (1999).
- 107 D. Denny-Brown and Royal College of Physicians of London., *The basal ganglia
and their relation to disorders of movement. Reprinted* (Oxford University Press,
London, 1963).
- 108 H. J. Freund, *Parkinsonism Relat Disord* **9**, 55 (2002).
- 109 A. M. Graybiel, *Rev Neurol (Paris)* **146**, 570 (1990).
- 110 C. D. Marsden and J. A. Obeso, *Brain* **117**, 877 (1994).
- 111 P. Brown, *Mov Disord* **18**, 357 (2003).
- 112 A. Raz, V. Frechter-Mazar, A. Feingold, M. Abeles, E. Vaadia, and H. Bergman,
J Neurosci **21**, RC128 (2001).

- 113 C. Bedard, H. Kroger, and A. Destexhe, *Physical Review E* **73** (2006).
- 114 N. K. Logothetis, *J Neurosci* **23**, 3963 (2003).
- 115 P. Brown, A. Oliviero, P. Mazzone, A. Insola, P. Tonali, and V. Di Lazzaro, *J Neurosci* **21**, 1033 (2001).
- 116 J. A. Goldberg, U. Rokni, T. Boraud, E. Vaadia, and H. Bergman, *J Neurosci* **24**, 6003 (2004).
- 117 Y. Goto and P. O'Donnell, *J Neurosci* **21**, 4498 (2001).
- 118 R. Levy, P. Ashby, W. D. Hutchison, A. E. Lang, A. M. Lozano, and J. O. Dostrovsky, *Brain* **125**, 1196 (2002).
- 119 J. M. Hurtado, C. M. Gray, L. B. Tamas, and K. A. Sigvardt, *Proceedings of the National Academy of Sciences of the United States of America* **96**, 1674 (1999).
- 120 R. Levy, W. D. Hutchison, A. M. Lozano, and J. O. Dostrovsky, *J Neurosci* **20**, 7766 (2000).
- 121 A. Priori, et al., *Neurol Sci* **23 Suppl 2**, S101 (2002).
- 122 D. Williams, A. Kuhn, A. Kupsch, M. Tijssen, G. van Bruggen, H. Speelman, G. Hotton, C. Loukas, and P. Brown, *Eur J Neurosci* **21**, 249 (2005).
- 123 D. Williams, A. Kuhn, A. Kupsch, M. Tijssen, G. van Bruggen, H. Speelman, G. Hotton, K. Yarrow, and P. Brown, *Brain* **126**, 1975 (2003).
- 124 D. Williams, et al., *Brain* **125**, 1558 (2002).
- 125 M. Cassidy, P. Mazzone, A. Oliviero, A. Insola, P. Tonali, V. Di Lazzaro, and P. Brown, *Brain* **125**, 1235 (2002).
- 126 A. A. Kuhn, T. Trottenberg, A. Kivi, A. Kupsch, G. H. Schneider, and P. Brown, *Exp Neurol* **194**, 212 (2005).
- 127 G. Foffani, A. Priori, M. Egidi, P. Rampini, F. Tamma, E. Caputo, K. A. Moxon, S. Cerutti, and S. Barbieri, *Brain* **126**, 2153 (2003).
- 128 L. M. Doyle, A. A. Kuhn, M. Hariz, A. Kupsch, G. H. Schneider, and P. Brown, *Eur J Neurosci* **21**, 1403 (2005).
- 129 W. Hauber, *Prog Neurobiol* **56**, 507 (1998).
- 130 W. Schultz, *Gen Pharmacol* **19**, 153 (1988).

- 131 R. Amirnovin, Z. M. Williams, G. R. Cosgrove, and E. N. Eskandar, *J Neurosci* **24**, 11302 (2004).
- 132 R. Levy, W. D. Hutchison, A. M. Lozano, and J. O. Dostrovsky, *J Neurosci* **22**, 2855 (2002).
- 133 P. J. Magill, J. P. Bolam, and M. D. Bevan, *Neuroscience* **106**, 313 (2001).
- 134 J. R. Walters, D. Hu, C. A. Itoga, L. C. Parr-Brownlie, and D. A. Bergstrom, in *The Basal Ganglia VIII*, edited by J. P. Bolam, C. A. Ingham and P. J. Magill (Springer Science and Business Media, New York, 2005), p. 37
- 135 R. M. Costa, *Annals of the New York Academy of Sciences* **1104**, 172 (2007).
- 136 R. M. Costa, S. C. Lin, T. D. Sotnikova, M. Cyr, R. R. Gainetdinov, M. G. Caron, and M. A. L. Nicolelis, *Neuron* **52**, 359 (2006).